



A review of common natural disasters as analogs for asteroid impact effects and cascading hazards

Timothy Titus¹ · D. Robertson² · J. B. Sankey³ · L. Mastin⁴ · F. Rengers⁵

Received: 29 June 2022 / Accepted: 15 November 2022 / Published online: 6 February 2023

This is a U.S. Government work and not under copyright protection in the US; foreign copyright protection may apply 2023

Abstract

Modern civilization has no collective experience with possible wide-ranging effects from a medium-sized asteroid impactor. Currently, modeling efforts that predict initial effects from a meteor impact or airburst provide needed information for initial preparation and evacuation plans, but longer-term cascading hazards are not typically considered. However, more common natural disasters, such as volcanic eruptions, earthquakes, wildfires, dust storms, and hurricanes, are likely analogs that can provide the scope and scale of these potential effects. These events, especially the larger events with cascading effects, are key for understanding the scope and complexity of mitigation, relief, and recovery efforts for a medium-sized asteroid impact event. This paper reviews the initial and cascading effects of these natural hazards, describes the state of the art for modeling these hazards, and discusses the relevance of these hazards to expected long-term effects of an asteroid impact. Emergency managers, resource managers and planners, and research scientists involved in mitigation and recovery efforts would likely derive significant benefit from a framework linking multiple hazard models to provide a seamless sequence of related forecasts.

Keywords Asteroid impact · Cascading hazards · Planetary defense · Integrated framework

✉ Timothy Titus
ttitus@usgs.gov

¹ Astrogeology Science Center, U.S. Geological Survey, Flagstaff, AZ, USA

² NASA Ames Research Center, Mountain View, CA, USA

³ Southwest Biological Science Center, Grand Canyon Monitoring and Research Center, U.S. Geological Survey, Flagstaff, AZ, USA

⁴ U.S. Geological Survey Volcano Observatory, Vancouver, WA, USA

⁵ Geologic Hazards Science Center, U.S. Geological Survey, Golden, CO, USA

1 Introduction

Modern civilization has no collective experience with possible wide-ranging effects from a medium-sized (300 m–1 km) asteroid impactor. The initial effects from an impact within this size range could result in a series of cascading hazards that extends far outside of the initially affected region and could continue to pose a threat to human activity for years.

This paper will review the hazards from an asteroid impact with particular focus on the long term, downwind, downstream, and cascading hazards. It will discuss analogs for these effects from other natural hazards with which we have more experience. Finally, it will discuss the potential differences between the analog and the asteroid impact effects, and gaps in the knowledge that will need to be filled in the future to develop better models for long-term asteroid impact hazard forecasting.

1.1 Motivation

While small meteor events are common, larger asteroid impact events luckily are not, with the probability of an impact event decreasing with increasing size (and the potential for devastating results). At the sub-meter size is comet debris that harmlessly burns up in the atmosphere, causing beautiful nighttime displays; meteor showers fall into this category. On the other end of the spectrum are large impactors (> 10 km) that result in extinction-level events, such as the Chicxulub impact that is believed to be responsible for the extinction of non-avian dinosaurs, 66 million years ago (e.g., Schulte et al. 2012). In between these endmembers, effects can range from shattered windows (e.g., the 2013 Chelyabinsk bolide event that caused a massive airburst) to regional devastation, with likely global effects on climate and air quality. Tunguska, the largest known impact in modern history was still relatively small, with damage largely restricted to a remote region of Siberia (Artemieva and Shuvalov 2016; Wheeler and Mathias 2019).

Considerable effort has been made to characterize effects from the impact of an asteroid. First-order effects are typically blast wave, thermal radiation, cratering, earthquakes, ejecta, and tsunamis (e.g., Hills and Goda 1993; Collins et al. 2005; Mathias et al. 2017; Stokes et al. 2017; Rumpf et al. 2017). These effects are nearly immediate and diminish with distance from the impact (or airburst) location.

Second-order effects may be triggered by the first-order effects, causing a cascade of hazards that may be time-delayed and propagate large distances from the initial damage zone. Figure 1 shows a diagram of these many interrelated causes and effects that result in cascading hazards. For small impactors, these delayed or displaced effects are likely to be negligible outside of the immediate impact area, i.e., the local area. For large impactors, these regional cascading effects may be overshadowed by global climate perturbations. Medium-sized impactors, however, can cause local devastation with secondary effects that ripple outward into regional communities over years, perhaps decades.

Simplistically, second-order effects can be thought of as either downwind, downstream, or occurring later. Asteroid impacts and airbursts spread debris from both the asteroid and from upthrown earth around an impact site. Airborne debris will blow downwind and land as fall deposits. Debris that accumulates in drainages may be washed downstream, aggrading river channels and inundating downstream areas as debris flows or sediment-laden floodwaters. While modern humanity has no frame of reference for cascading effects from a medium-sized asteroid impact, we are familiar with more common natural hazards, such

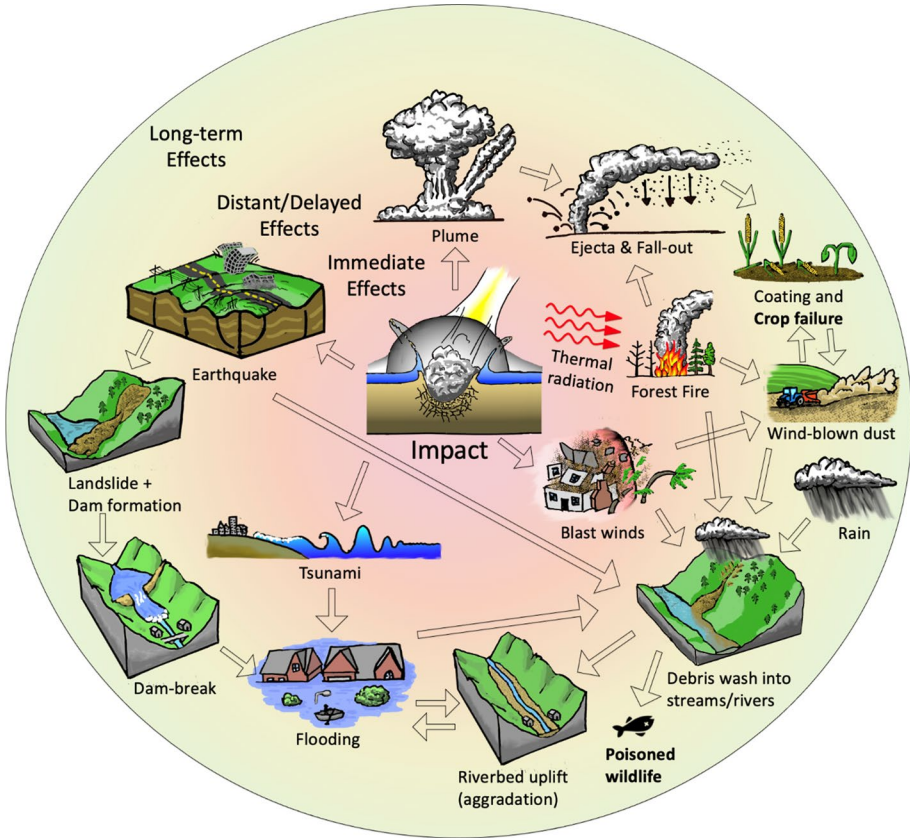


Fig. 1 A graphical abstract that shows the interconnectedness of cascading hazards from an asteroid impact scenario. In general, the cascading hazards are displaced in space or time as one moves out from the center of the circle. Multiple feedback processes occur. Often the timing of the hazard is triggered by rain or snowmelt events. While not specifically noted in the diagram, poisoned wildlife or crop failure will impact human communities through reduced food security, tainted drinking water, and economic impact.

as volcanic ash, dust plumes, wildfires, debris flows and floods. Many of these more common natural hazards are part of the cascading effects that one may expect from a medium-sized impactor. If we can connect these effects, mostly through models, we can start to answer some key questions, such as: What is the size range for a medium-sized impactor where these effects become important? What are the effects that emergency managers should be planning to mitigate? What will be the timescale, cost, and level of effort for long-term recovery of the region? How large of a region is affected by second and third-order cascading effects? Currently, we are only able to answer these questions in the broadest context, but more detailed answers specifically tied to impactor locations will need to be interlinked and coupled with hazard models as described throughout this paper.

1.2 Background

In 2018, the White House released a National Near-Earth Object Preparedness Strategy and Action Plan (NSTC, 2018; hereafter called the Action Plan). This plan provides a framework for both agency and interagency coordination efforts to plan and prepare for possible future asteroid impacts. In the Action Plan, five goals were established: (1) enhance near-earth objects (NEO) detection, tracking, and characterization capabilities; (2) improve NEO modeling, predictions, and information integration; (3) develop technologies for NEO deflection and disruption missions; (4) increase international cooperation on NEO preparation; and (5) strengthen and routinely exercise NEO impact emergency procedures and action protocols. Each goal contains several actions and a list of lead and supporting agencies.

In this paper, we focus on Goal 2. The specific action items listed to achieve Goal 2 are as follows: (2.2) Ascertain what information each participating organization requires on what timeframe, identify gaps, and develop recommendations for modeling improvements; (2.4) Establish a suite of computer simulation tools for assessing the local, regional, and global risks associated with an impact scenario; (2.6) Continually assess the adequacy and validity of modeling and analysis through annual exercises, test problems, comparison to experiments, and peer review activities. In addition, this paper provides a range of possible cascading hazards that should be considered when implementing response and recovery actions necessary to save lives, mitigate suffering, and limit property damage.

In an ideal world, the astronomers would identify any hazardous objects in sufficient time for the spacefaring nations to successfully deflect the objects, rendering a civil defense response moot, except in cases of small or remote events where civil defense would be less expensive and easier to implement. The world is not ideal, and we have yet to identify all potentially hazardous objects (PHO) above a minimum size that could cause damage. The Chelyabinsk airburst is a case in point. Even if an object is identified as earthbound, there may not be sufficient time to launch deflection missions. Even if deflection missions are launched, successful deflection is not guaranteed. As such, civil defense and post-impact recovery efforts must remain on the table. Mitigation efforts should be understood well in advance of the actual event.

1.3 The complexity of multi-hazard risk assessment and cascading effects

The impact of a medium-sized asteroid will not be a single natural hazard that can be treated as an event that only affects a well-defined area over a short period of time. Instead, the initial hazard will result in a series of cascading effects. Emergency plans will need to consider the complexity of multi-hazard risk assessment and cascading effects. Modeling and monitoring will be needed to reduce the risk that human actions actually exacerbate effects, instead of mitigating them.

The 2008 Wenchuan earthquake in China provided an example of a natural hazard where the initial damage was compounded by cascading effects, such as debris flows, landslide dams, and increased potential for flooding for years to come (e.g., Fan et al. 2021). Volcanic eruptions provide another relevant analog where the multi-hazard risk remains for years, once again, compounded by cascading effects such as lahars (volcanic debris flows). Also analogous are wildfires that are dangerous for humans who are in the immediate path of the flames, those who are downwind where smoke accumulates, as well as much later

in time for humans who rely on water and soil that is polluted by toxins from combusted materials, or who live downslope from burned hillslopes that are dangerous flooding or landslide hazards each time it rains.

To add to the complexities of understanding the potential for cascading effects from an impactor, is that any impact scenario during this century will occur within the context of a changing global climate. Global climate change causes greater weather extremes that drive cascading hazards like floods, fires, and landslides (Duncombe 2021, and references therein). While addressing climate change and extreme weather is beyond the scope of this paper, it does support the idea that natural hazards are modified by the environment at the time.

1.4 Review outline

Section 2 describes our current understanding of the initial effects from either an asteroid impact or airburst. Section 2 also includes a review of what is known about the largest impact in recorded history, the 1908 Tunguska impact. Section 3 reviews a series of natural hazards that should be considered as analogs for at least some of the longer-term hazards from a medium-sized impact event. This section addresses the current state of models used for these analog hazards, discusses how they can be applied to better understand cascading effects, and enumerates the unknowns in attempts to couple these models. The natural hazards discussed are (1) volcanoes, (2) dust storms, (3) wildfires, (4) earthquakes, and (5) hurricanes. Section 4 discusses cascading hazards within the context of the human impact, climate change and the need for an integrated forecasting framework. Section 5 concludes with a summary.

2 Review of the immediate effects (current state of the art)

As an asteroid passes through the atmosphere, it creates a shock wave in front that compresses and heats the air to tens of thousands of degrees Celsius. Asteroids smaller than 100 m in diameter typically break up in the air due to the pressure. As the fragments spread out, they are decelerated more rapidly by the atmosphere and heat the atmosphere at a very high rate (Robertson and Mathias 2019; Shuvalov et al. 2013; Wheeler et al. 2017). Larger or metallic asteroids typically impact the ground. Compressive heating from the impact will vaporize the asteroid and a portion of the ground. In either the airburst or cratering case, the hot, high-pressure air and rock vapor cause the two main damage mechanisms: a blast wave and thermal radiation. Impacts into the ocean can also cause tsunami waves to propagate out from the impact site and cause damage at long distances, and similarly, for impacts into the ground, seismic waves propagate out and cause damage even before the blast wave arrives. In the case of extremely large impacts, such as the Chicxulub impact, large pieces of debris can be ejected out into space and cause subsequent meteors as they fall back down into the atmosphere at other locations around the globe (Kring and Durda 2004). The immediate effects will be described more below.

2.1 Blast overpressure

As in a conventional explosion, the rapid deposition of energy greatly increases the pressure, which drives the air away from the explosion in a blast wave. The shock wave and following hurricane force winds can flatten trees (Fast 1967; Jenniskens et al. 2019) and knock down buildings close to the impact site (Glasstone and Dolan 1977). Further out, the blast can shatter windows and send glass shards flying as hazardous projectiles, as seen in the Chelyabinsk event where ~1500 people were sent to the hospital, mostly with lacerations due to flying glass (Popova et al. 2013). Damage is typically inferred from the blast overpressure or wind speed using known damage relations from nuclear bombs (Glasstone and Dolan 1977), other large explosions (Mannan 2005), or hurricanes (Lindell et al. 2006).

Of the various immediate effects of an asteroid impact, the blast wave is typically the most damaging and usually determines the expected casualties and (or) the area that would need to be evacuated prior to impact (Collins et al. 2005; Mathias et al. 2017; Rumpf et al. 2017; Glazachev et al. 2021). Consequently, the blast is probably the most studied aspect of asteroid impacts. The blast wave is usually either calculated from semi-analytical models or from high-fidelity hydrocodes. Semi-analytical models generally fall into a couple of categories: (1) “pancake” semi-analytic models which treat the meteor as a cloud of debris that flattens and spreads out like a pancake (Hills and Goda 1999; Chyba et al. 1993; McMullan and Collins 2019); (2) discrete fragmentation semi-analytic methods, which model the progressive fragmentation of the meteor into smaller and smaller fragments which are treated independently (Passey and Melosh 1980; ReVelle 2007); and (3) hybrids of the previous two types (Wheeler et al. 2018). Hydrocode simulations have difficulty modelling at both the centimeter-scale resolution required to capture the meteor fragmentation down to typical meteorite scales and the hundreds-of-kilometers scale required to model long-range propagation of the blast wave. Currently, most hydrocode simulations straddle these two regions (Boslough and Crawford 1997; Jutzi et al. 2015), or they are split into close-in simulations that calculate the break-up and energy deposition into the atmosphere (Shuvalov et al. 2017; Robertson and Mathias 2019; McMullan 2020) and far-field simulations where the energy emanates from a region about the size of the meteor or larger (Aftosmis et al. 2016). Accurate simulation of all scales, and hence the efficiency of energy transfer from meteors to blast waves, should be possible in the future with ever-improving computational resources.

There may be long-term effects from the debris created from the blast wave, some of which may contain toxic materials, seep into groundwater, wash into nearby rivers, or blow downwind. These possible long-term effects are discussed within the context of more frequent natural disasters in Sect. 3.

2.2 Thermal effects

The hot layer of air from entry radiates energy to the ground (Collins et al. 2005; Popova et al. 2020; Johnston et al. 2018; Svetsov et al. 2020). In the case of ground impacts, a large plume of extremely hot material typically travels back up the evacuated entry corridor that the asteroid just punched in the atmosphere. If the entry angle is shallow, the plume will rise vertically due to buoyancy of the hot vapor rather than up the entry corridor (Artemieva et al. 2019).

The best current observational analogs for the thermal radiation are the measurements from nuclear bomb tests in the 1950s and 60 s. There are some important differences though. Nuclear bombs are essentially point sources with the energy released within a few meters, whereas an airbursting asteroid's energy may be spread over tens of kilometers passage through the atmosphere. The temperatures in the blast from nuclear bombs are also much higher, reaching into the millions of degrees Celsius, and up to 50% of a nuclear bomb's energy may be released as radiation in the form of gamma rays (Glasstone and Dolan 1977). Meteor plumes may reach thousands of degrees Celsius, with only a few percent or less of the energy emitted as radiation typically in the ultraviolet down to infrared (Svetsov and Shuvalov 2017; Coates et al. 2021).

Modern hydrocode simulations of asteroids have recently examined asteroid impacts in more detail (Johnston and Stern 2019; Svetsov et al. 2020). Spectral radiation codes which calculate the emission spectra of vaporized rock and ionized air can determine from first principles the fraction of kinetic energy the meteor emits as radiation (luminous efficiency), rather than relying on an analog.

At locations near a ground impact or a low-altitude airburst, due to hot air flow or radiation, temperatures may exceed that for melting sand, resulting in Libyan desert glass such as found in one of Tutankhamun's brooches. This is similar to trinitite glass found underneath nuclear bomb tests which were conducted over sand in New Mexico and Nevada (Boslough and Crawford 2008). Further away, the radiation may cause grass fires and other wildfires (Melosh et al. 1990; Collins et al. 2005; Robertson et al. 2017a, b); the Tunguska event apparently caused a wildfire that burned 500 km² of Siberian taiga (boreal forest) for example (Zenkin and Ilyin 1964; Johnston and Stern 2019).

Long-term effects from thermal radiation relate to debris left by fires, and from particles and chemicals lofted into the air in smoke plumes. These possible long-term effects are discussed within the context of more frequent natural disasters in Sect. 3.

2.3 Tsunami waves

If an asteroid hits the ocean, the resulting tsunami can potentially damage areas farther away than areas affected by the blast wave or thermal radiation. Analytical models of impact tsunami waves (Chesley and Ward 2006) coupled crater scaling laws (Schmidt and Holsapple 1982) to wave propagation models of explosion-generated waves (Van Dorn et al. 1968). Hydrocode simulations of impacts (Robertson and Gisler 2019) show only 1–2% of the energy being transferred to travelling waves, suggesting tsunamis resulting from impacts are less hazardous than previously estimated. As the initial transient crater in the water rebounds, it sends up a large central jet (Worthington and Cole 1900), which in turn collapses in a highly turbulent, chaotic manner. Large waves are pushed out from the lip of the crater and the collapse of the central jet, and initially form breaking-waves, which further dissipate the energy before a smooth-travelling wave is established (Wünnemann et al. 2010).

Unless an impact is extremely large or onto a continental shelf, waves from an impact will have wavelengths comparable to the depth of the ocean or shorter. For such deep-water waves, the wave speed depends on wavelength, so the wave disperses as it travels and the amplitude decays as $1/r$ for radial distance r (Van Dorn et al. 1968). In contrast, the wavelengths for earthquake tsunamis are typically tens or hundreds of kilometers and are, therefore, shallow water waves where all frequencies travel at the same speed, the wave retains

its shape, and the amplitude decays as $1/\sqrt{r}$ (Le Mehaute and Wang 1996; Berger and LeVeque 2018).

As waves from the deep ocean approach shore, the water depth decreases which causes waves to slow down and shorten in wavelength but get taller in height, thus increasing the steepness. Once the wave height approaches the water depth, the wave will break. This makes earthquake tsunamis dangerous, as what was a long but small swell in deep water, becomes a wall of water which inundates the coastline. This will also happen for impact tsunamis, but due to their shorter wavelength and greater height, this may happen as the wave propagate onto the continental shelf, rather than the beach. The continental shelf in many places around the world extends up to hundreds of kilometers offshore allowing much more time and distance for the waves to dissipate before reaching shore (Khazins and Lynett 2005).

Once an impact tsunami wave becomes a shallow water wave, either due to impact in shallow water, or breaking as a wave nears the shore, propagation and inundation can be efficiently calculated since the wave does not vary with depth (Le Mehaute and Wang 1996; Korycanski and Lynett 2007; Berger et al. 2011). Flood fatality risk varies mostly with flooding depth (Jonkman et al. 2008; Koshimura et al. 2009).

Long-term effects are mostly related to debris and mobilization of pollutants. These possible long-term effects are discussed within the context of more frequent natural disasters in Sect. 3.

2.4 Earthquake effects

Earthquakes caused by asteroid impacts have been less studied, since the blast wave is typically expected to be more damaging at a given distance. Recent simulations showed the earthquakes induced by airbursts were of minimal threat due to low efficiency of coupling the blast waves to ground waves (Svetsov et al. 2017). For ground impact cases, the energy converted into travelling waves is very small (0.01–0.1%) (e.g., Toon et al. 1997; Khazins et al. 2018), but may still cause damage comparable to the blast waves (Robertson et al. 2017a, b). Damage from seismic waves is generally proportional to peak ground vertical acceleration or velocity (Wald et al. 1999; Atkinson and Wald 2007).

Seismic waves travelling at 2–6 km/s will generally arrive before blast waves travelling at about 0.3 km/s, unless directly under the path of a low entry-angle impact. For very large impacts such as the Chicxulub impact, earthquakes were believed to have induced landslides and tsunamis at a distance before the arrival of ejecta or the main tsunami wave (Bralower et al. 1998; DePalma et al. 2019). Earthquakes, therefore, have the potential to be significant force multipliers if they trigger collapse of unstable slopes, causing domino effects, possibly more hazardous than the direct effects at a distance from the impact.

2.5 Plumes and atmospheric effects

For the purposes of this discussion, plume refers to any material deposited or lofted into the atmosphere, either in or back up the wake of entry, vertically under buoyancy, ejecta from ground impact, or more generally from events like smoke from fires, and volcanic eruptions. While plumes provide dramatic images, they are not a significant hazard until the volume of material deposited in the atmosphere and the fallout from it have a noticeable effect on crops downwind. At the extreme end, effects on the climate are the dominant hazard from multi-kilometer asteroids (Bardeen et al. 2017).

On the smaller and more frequent end of the asteroid impact probability distribution, the impact of an asteroid with ~3 kilotons equivalent of TNT in June 2018 just south of Moscow, caused bright noctilucent clouds over Russia and Europe for the next week or two (Ugolnikov and Maslov 2019). The impact of a ~20 m-diameter asteroid over the city of Chelyabinsk in February 2013, with ~500 kT, created a dust belt in the upper stratosphere which lasted for a few months (Gorkavyi et al. 2013) but with no significant effect on crops or waterways.

The Tunguska meteor of 1908, estimated to have been about 10 megatons (Artemieva and Shuvalov 2016; Wheeler and Mathias 2019), is the largest recorded airburst in modern times. No known asteroid with a diameter larger than 100 m has impacted the earth's surface within recorded history. Dust and (or) ice deposited into the atmosphere by the meteor airburst caused "white nights" for a week or so over all of Europe and Asia to the west of Tunguska (Witchell 1938; Kaufman 1908). Whether the meteor was a mostly rocky asteroid or a mostly icy comet is still a matter of debate, but simulations of the impact show the matter being ejected back up the evacuated entry corridor into space over a region from 100 to 400 km altitude and collapsing back to 100–300 km altitude to form a 1000-km-diameter cloud, which then spread around the world (Artemieva et al. 2019; Boslough and Crawford 2008). The particle size determines whether aerosols from the airburst stay lofted in the atmosphere or rain down to earth, and icy crystals are much better reflectors of sunlight than dust. Particles at 300-km altitude would be in direct sunlight over the north pole anywhere in Europe during midsummer, and particles at 100 km could scatter light from more northerly latitudes, similar to Polar Mesospheric Clouds which appear noctilucent (glowing at night; Thomas and Olivero 1986). Given that the Tunguska impact occurred in the Siberian taiga, sparsely inhabited by reindeer herders and a few scattered villages, there is no record of local or regional effects of dust fallout from the airburst on crops and rivers. Curiously, but not yet generally accepted, it has been speculated to have increased the annual growth of trees over a wide area to the North of the impact as far as the Arctic Ocean and is presumed to be due to fallout of nitrogen oxides acting as fertilizers (Kasatkina and Shumilov 2007).

2.6 Selection of currently used models of impact effects

There are many analytic (algebraic) models for the different impact-related phenomena in the literature, which are combined into complete hazard/risk models, a few of which are given below. NASA's Probabilistic Asteroid Impact Risk (PAIR) model (Mathias et al. 2017) also includes a couple of semi-analytic models which require the solution of Ordinary Differential Equations. These compendium models are typically designed to be fast running, so they can be run millions of times over distributions of entry parameters to deal with cases of incomplete information such as in the tabletop exercises of planetary defense (e.g., <https://cneos.jpl.nasa.gov/pd/cs/pdc21/>).

At higher fidelity, hydrocodes provide a tight coupling of fluid dynamics and solid mechanics, and solve partial differential equations of conservation equations, and material states. These take days if not weeks to run on supercomputers for a single impact case but provide our best estimates of the effects and can be used to improve the analytic models. Again, there are many such models including both Eulerian (fluid-like) and Particle codes, and just a few have been noted (Table 1).

Finally, there are a few specialized high-fidelity simulations worth noting that expand the capabilities of current hydrocodes. Computational Fluid Dynamic (CFD) simulations can propagate blast waves or tsunami waves more efficiently than hydrocodes. They are, therefore,

Table 1 List of examples of models used to determine the initial effects of an asteroid airburst or impact. This list is not meant to be exhaustive

| Model | Fidelity | Blast | Thermal | Crater | Ejecta | Seismic | Tsunami | Climate | Reference | Comments |
|------------------------------------|--------------------------------------|-------|---------|--------|--------|---------|---------|---------|----------------------------|---|
| Probabilistic Asteroid Impact Risk | Analytic/semi-analytic | X | X | X | X | X | X | X | Mathias et al. 2017 | |
| Impact Earth | Analytic | X | X | X | X | X | X | X | Collins et al. 2005 | https://impact.esc.ic.ac.uk/ImpactEarth |
| Asteroid Hazard | Analytic | X | X | X | X | X | X | X | Popova et al. 2020 | http://www.asteroidhazard.pro/ |
| ALE3D | Hydrocode | X | X | X | X | X | X | X | Robertson and Gislser 2019 | |
| SOVA | Hydrocode | X | X | X | X | X | X | X | Shuvalov et al. 2017 | Gray-body radiation approximation |
| iSALE | Hydrocode | X | | X | | X | | | Collins et al. 2020 | |
| HARA | Line radiation (High fidelity) | | X | | | | | | Johnston et al. 2018 | Line-by-line radiation model |
| GeoCLAW | Shallow water solver (High fidelity) | | | | | | X | | Berger and LeVeque 2018 | Not appropriate for transient impact craters shallower than the water |
| CESM | Fluid dynamics (High fidelity) | | | | | | | X | Bardeen et al. 2017 | https://www.cesm.ucar.edu/ |

particularly useful in modeling the predominant blast hazard (Aftosmis, 2019). Spectral-line radiation models, such as the High-temperature Aerothermodynamic RADIation (HARA) model, improve upon the thermal transport models in most hydrocodes which use a black-body radiation diffusion approximation. Shallow water solvers such as GeoCLAW are suitable for impacts into shallow water or when waves reach the shore and can provide high-fidelity inundation estimates much faster than a hydrocode or CFD simulation. Finally global climate models such as Community Earth System Model (CESM) can calculate the effects on the climate from kilometer- scale asteroids. Additional details can be found in Table 1.

3 Review of common natural hazards as analogs

Asteroid impacts are expected to cause multiple cascading effects—ranging from the initial thermal radiation, overpressure blast waves, earthquakes, and plumes to cascading hazards such as fires, floods, debris flows, and so on. A variety of Earth phenomena have produced analogous hazards. Volcanic activity may come the closest to replicating many of the initial and cascading effects, as well as the size and scope of regional devastation. Large earthquakes also replicate cascading hazards on a region scale. In this section, we discuss these natural hazards, as well as cascading hazards, within the context of planetary defense.

3.1 Volcanoes

Volcanic eruptions can produce lahars, lava flows, pyroclastic flows, ash clouds, shock waves, and ballistically ejected blocks that resemble asteroid-produced phenomena (Fig. 2). Secondary effects, such as resuspended ash, remobilized lahars, and global cooling, can cause problems for years or decades.

The hazards posed generally scale with the size of the eruption, which is quantified using the volcanic explosivity index or VEI (Newhall and Self 1982), which considers both the volume of erupted material and the rate of ejection. Explosive eruptions eject

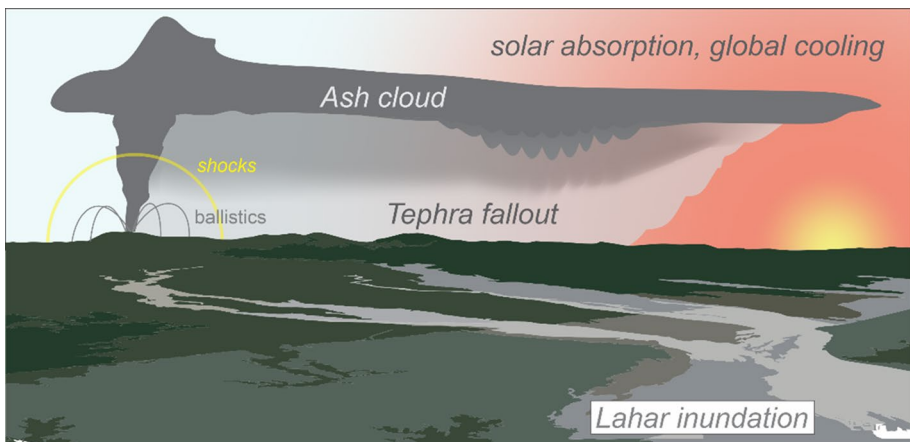


Fig. 2 Illustration of key volcano hazards that are relevant to hazards of asteroid impacts. It should be noted that the ash clouds can reach the stratosphere, resulting in global cooling effects

fragmental debris, known as tephra, into the atmosphere. Tephra finer than 2 mm diameter is termed ash. Most tephra falls downwind to form tephra-fall deposits. Eruptions of VEI 4, 5, 6, and 7, for example, have tephra-fall volumes that exceed, 0.1, 1, 10, and 100 km³, respectively. Because tephra contains bubbles, the dense-rock equivalent (DRE) volume of magma required to produce a cubic kilometer of tephra is approximately one fourth to one half the tephra volume itself. Plume heights of VEI 4 and ≥ 5 eruptions typically exceed 10 km and 25 km, respectively; thus VEI 5 and larger eruptions almost always inject ash and gas into the stratosphere. Large eruptions are less frequent than small ones, and global recurrence times for VEI 4, 5, 6, and 7 events are roughly a year, a decade, several decades, and a few centuries, respectively.

3.1.1 Examples of some large historical eruptions and their effects

“Mount Tambora” (Gunung Tambora), Indonesia, 1815, (VEI 7) erupted about 50 km³ of magma, making it perhaps the largest eruption in recorded history. Ash and ~60 Mt sulfur dioxide were ejected to an altitude of at least 43 km, producing a global sulfate aerosol veil that enhanced sunsets in North America (Stothers 1984), reduced global temperatures, caused wintry temperatures in North America in July, and resulted in widespread crop failures. At least 71,000 people died, mostly from indirect effects such as crop failure and disease (Oppenheimer 2003).

Krakatau, Indonesia, 1883, (VEI 6) erupted about 26 km³ magma from a small volcano-island in the “Sunda Strait” (Selat Sunda) (Simkin and Fiske 1983). Eruption columns repeatedly collapsed onto the water surface around the island, producing tsunamis that propagated to nearby shorelines. About 36,000 people died (Verbeek 1885), the great majority by tsunamis. A few thousand were killed by pyroclastic flows (Self and Rampino 1980). Global temperatures dropped by about a half degree Celsius for a few years following this event (Angell and Korshover 1985; Bradley 1988).

Mount Saint Helens, Washington (USA), 1980, (VEI 5) erupted about 0.25 km³ of magma on May 18, 1980 (Lipman and Mullineaux 1981). From late March through May 18, 1980, a magma body intruded into the upper edifice of the volcano, destabilizing it, and producing hundreds of small steam eruptions. At 8:32 AM local time on the morning of May 18, a magnitude-5.2 earthquake caused the north flank of the volcano to slide away, exposing the magma body, which expanded northward as a lateral blast that killed 57 people. This blast was followed from about 09:00 AM to 05:30 PM by a sustained Plinian eruption that sent about a cubic kilometer of tephra across Washington State (Sarna-Wojcicki et al. 1981). Tephra from that eruption closed a large section of the main highway, Interstate 90, for most of a week. Business districts in several downwind cities and towns were closed for days (Warrick et al. 1981), resuspended ash caused increases in hospital visits for weeks (Bernstein et al. 1986), and one community was forced to shunt raw sewage into the nearby river when the sewage treatment plant was clogged with sediment (Schuster 1981). On May 18, west of the mountain, large debris flows destroyed many houses and bridges, and forced the closure of the main north–south highway, Interstate 5, for a day (Foxworthy and Hill, 1982).

El Chichón, Mexico, 1982, (VEI 5) erupted about 0.5 km³ magma on March 29 and April 4, 1982. Ejections on March 29 sent tephra-fall ENE in the troposphere and WSW in the stratosphere. Ejections on April 4 produced eruptive columns that repeatedly collapsed to form pyroclastic density currents that devastated a roughly circular area up to 6 km from the vent (Carey and Sigurdsson 1986). Nine villages were partially or completely

destroyed, and loss of human life was perhaps as high as 2000. A cloud containing 7–8 Mt SO₂ (Varekamp et al. 1984) circled the globe, cooling temperatures by perhaps 0.1–0.2 °C for a few years (Dutton and Christy 1992).

Mount Pinatubo, Philippines, 1991, (VEI 6) erupted about 6–10 km³ magma over a 9-h period, producing a 35–40 km high plume and an umbrella cloud that expanded to about 1,000 km diameter (Koyaguchi and Tokuno 1993). About 320 people died in the eruption, mostly from roof collapse as heavy tephra fall was further weighed down by rainwater from Typhoon Yunya (Pinatubo Volcano Observatory Team 1991). Evacuation of 58,000 residents within 30 km a few days before the eruption prevented more loss of life. An additional ~200,000 fled the area in the days following the main event. Thick debris that accumulated on the flanks of the volcano was remobilized in lahars for many years. By fall of 1991, nearly every bridge within 30 km of the volcano had been destroyed. Several towns within that distance had been partially buried, and most within 50 km were threatened with flooding or burial (Pinatubo Volcano Observatory Team 1991). About 100,000 people were living in evacuation camps and 700 had died from secondary effects. Damage to crops, infrastructure, and personal property totaled at least \$US 374 million in 1991 (\$US 813 M adjusted for inflation as of 2022), and an additional \$US 69 million in 1992 (\$US 146 M adjusted for inflation as of 2022) (Mercado et al. 1995). The injection of about 20 Gt of SO₂ cooled global temperature by about a half degree Celsius for a few years (Self et al. 1996). For reference, estimates give the equivalent asteroid impact as one with ~3 Gt energy which is equivalent to ~350 m in diameter (Toon et al. 1997).

3.1.2 Main hazards of eruptions that are relevant to asteroid impacts.

The main hazards of eruptions that are relevant to asteroid impacts are as follows:

Airborne debris dispersal is among the most widespread of hazards. The more material that is ejected, the greater the effects. Eruptions > 5 on the VEI (Newhall and Self 1982), such as Mount Saint Helens (1980), El Chichón (1982), or Pinatubo (1991) occur about once per decade globally. They eject 1–10 km³ of tephra, and can deposit centimeters or more of ash hundreds of kilometers downwind. Eruptions of VEI 6, such as Mount Pinatubo (1991) or Mount Katmai, Alaska (1912) expel 10–100 km³ tephra, occur globally once or twice per century, can deposit more than a meter of ash within a few tens of kilometers, and can bury fields and towns over the following decades with remobilized sediment (Gran et al. 2011). Stratospheric sulfur dioxide emitted from Pinatubo reduced global temperatures by about a half degree through stratospheric ejection of SO₂ (Self et al. 1996). Eruptions of VEI 7, such as Tambora (1815) eject 100–1000 km³ of tephra, recur over timescales of millennia, and can cause widespread devastation and crop failures on distant continents due to global cooling. VEI 8 eruptions, known as supereruptions, eject > 1000 km³ tephra, recur over time scales of ~10⁵ years, and can be globally devastating (Sparks et al. 2005).

Ashfall impacts include aggravated breathing problems, damage to electronics and machinery, power outages, reduced traction on roadways, and collapse of roofs when thick. The impact of different amounts of ashfall is hard to quantify, but ashfall thicknesses greater than several centimeters were sufficient to collapse roofs at Pinatubo and Galunggung (Spence et al., 1995; Blong 1984). Ashfall thickness of 1 mm or so causes a measurable reduction in roadway traction (Blake et al. 2017). Thicknesses of several millimeters or more have caused flashover of electrical transformers, especially when ash is wet (Wilson et al. 2012). And even thin dustings of ash can reduce visibility or make breathing

uncomfortable. Ashfall of 200 g/m^2 was sufficient to prompt city managers in Missoula, Montana to shut down the business district for a few days in 1980 (Warrick et al. 1981). This mass load corresponds to a thickness ranging from a few millimeters if ash is fresh and newfallen, to tenths of a millimeter if compacted by rainfall (Sarna-Wojcicki et al. 1981). Ashfall as low as 1 g/m^2 is noticeable on car windshields and can prompt residents to take precautionary measures.

Effects on agriculture depend on many factors; for example, ash can increase runoff in areas that have intense rainfall, or increase erosion in non-tilled farmland if less cohesive than the local soil (Nammah et al. 1986). North of Crater Lake, Oregon, thick deposits of coarse pumice do not hold moisture, inhibiting plant growth (Williams 1942). In other places, thinner deposits of loamy grain-size can improve drainage and add micronutrients (Cook et al. 1981). Crop damage from ashfall can vary greatly depending on the crop type and season. Crops like alfalfa with broad horizontal leaves are more prone to ash-loading damage than those with vertical stalks, like wheat. The May 18, 1980 eruption of Mount Saint Helens deposited centimeters of ash over wheat fields in central Washington, but early in the growing season, the vertical stalked wheat was not significantly damaged. Ash did, however, kill many grasshoppers, which made spraying unnecessary in Grant, Douglas and western Lincoln Counties (Cook et al. 1981). A smaller eruption on June 12 sent a few millimeters of ash southwest, into fields of nearly ripe raspberries. The raspberries could not easily be cleaned of ash, resulting in a 75% crop loss in Clark County (Cook et al. 1981).

Volcanic shock waves occur primarily during small explosions and occasionally break windows within several kilometers distance (Morrissey and Mastin 2000; Nairn 1976). Eruptions also produce infrasonic pressure waves as air is displaced from the vent. During large eruptions, for example, as occurred at Mount Saint Helens in 1980 (Reed 1987) and Krakatau in 1883 (Verbeek 1885), large pressure anomalies developed as huge volumes (10^8 – $10^{11} \text{ m}^3/\text{s}$) of ash and gas were ejected. These outward propagating anomalies had a frontal gradient that sharpened with distance to produce sonic boom sounds at distances beyond a few hundred kilometers. Sonic boom sounds from Mount Saint Helens, for example, were heard 300 km away in Victoria, B.C. but not within 100 km (Fairfield 1980). The air waves at Krakatau in 1883 were audible to distances beyond 4000 km. Airwave amplitudes at Saint Helens and Krakatau match those produced during explosive detonations of a few megatons TNT equivalent (Reed 1987) and 100–150 Mt, respectively (Harkrider and Press 1967). Despite their high energy, there were few reports of damage from volcanic airwaves. An important exception was the extensive tree blowdown at Mount Saint Helens on May 18, 1980, which resembled photographs at Tunguska in 1908 (Robertson and Mathias 2019). The Mount Saint Helens blowdown was produced by a dusty gas mixture whose momentum was proportional to gas density times velocity; hence, high air density as well as wind speed were responsible. Controversy has swirled over whether shock waves or gravitational column collapse was more important in producing the treefall (Kieffer 1981; Waitt 1981).

Ballistic Blocks are also ejected from volcanic craters in a manner analogous to those at meteorite impact sites. Volcanic ejection distances do not typically extend more than 5–10 km (Taddeucci et al. 2017), whereas impactor ejecta can travel 100 s of km or even be ejected into space (Kring and Durda 2002). The maximum thickness of ejecta as a function of distance from the impact center should typically decrease as a function of that distance to the -3 power (Collins et al. 2005). The thickness is also a function of the volume of regolith excavated by the impact and, therefore, also scales with crater radius.

Global cooling during big eruptions is due to stratospheric sulfur gases, which transform into sulfate aerosols that absorb solar radiation or scatter it back into space (Robock 2000). Most fine ash from big eruptions is thought to be removed from the atmosphere within days and only plays a minor role in cooling (Niemeier et al. 2009). Historical data have established a relationship between eruption size and SO₂ release, and documented the effect of these eruptions on sun-blocking properties such as aerosol optical depth (e.g., Carn et al. 2016; Myhre et al. 2013). Prehistoric sulfate layers in ice cores correlate with periods of global cooling inferred from tree-ring studies, and with periods of known famine and plague, e.g., around 541–543 C.E. in Europe (Sigl et al. 2015).

In unusual circumstances, asteroid impacts may release SO₂, such as when the Chicxulub meteorite plunged into an anhydrite deposit (Brett 1992). However, asteroid impacts generally do not release sulfur gases. Rather, global cooling following those impacts is assumed to be driven by fine (< 1 μm) stratospheric dust particles kicked up by the impact (Covey et al. 1994), or by soot from fires (Bardeen et al. 2017). The importance of these two mechanisms depends on how much of these materials are injected, and how long they remain. Alvarez et al. (1980) estimated about 10¹⁶ kg of dust settled out of the air to produce the K-T boundary layer. Smaller airburst events like Tunguska have produced noctilucent clouds that suggest debris dispersal at several tens of kilometers altitude (Gladysheva 2012). But if fine ash settles rapidly after volcanic eruptions, why would fine dust persist following impact events? Recent studies suggest that soot from fires persists longer (e.g., Khaykin et al. 2020). Wolbach et al. (1990) noted global black carbon deposits at the Cretaceous-Tertiary boundary, and inferred that worldwide fires following the Chicxulub impact injected 150,000 Tg of soot into the atmosphere. Global climate modeling found that a much smaller injection of 150 Tg soot would produce below-freezing temperatures over much of the northern hemisphere in summer (Coupe et al. 2019). Pankhurst (2022) also suggests that impacts into ground that are rich in K-Feldspar cause more climate change than impacts into other rocks because K-Feldspar is particularly efficient at nucleating ice formation.

3.1.3 Key parameters that control the amount and areal distribution of airborne debris

The key parameters that control the amount and areal distribution of airborne debris include:

3.1.3.1 Volume of debris Large eruptions with recurrence intervals of 10¹–10⁵ years produce 10⁰–10³ km³ of airborne debris; Asteroid sizes with the same impact recurrence intervals have volumes of 10⁻⁵–10⁻¹ km³ (diameters 60 m–1.2 km) (Toon et al. 1997). Thus, the volume of asteroids themselves is insignificant compared to the volume of large volcanic eruptions. But the amount of earth material ejected by an impact will increase the airborne volume by typically an order of magnitude or possibly up to two orders of magnitude (Toon et al. 1997). While a 60-m asteroid may well airburst and only deposit 10⁻⁵ km³, equivalent to a zero VEI, a metallic and likely ground impact object could eject up to 10⁻³ km³, equivalent up to VEI 2. The 1.2-km asteroid is guaranteed to impact the ground and would likely be the equivalent of VEI 5. For the Chicxulub impactor, based on the KT clay layer Toon et al. (1997) estimated the ejected molten rock at 25,000 km³, equivalent to VEI 9, which is larger than any single volcanic eruption.

3.1.3.2 Dispersal height Volcanic plumes rise due to buoyancy. Larger eruptions and (or) higher mass eruption rates produce higher plumes (Carey and Sigurdsson 1989; Wilson et al. 1978), up to about 45–50 km, where the thermal gradient in the stratosphere inhibits further rise. The same physics will limit the buoyant rise height of asteroid debris from shallow impacts such as the Chelyabinsk meteor (Popova et al. 2013). However, for steeper impacts, the debris is drawn up the evacuated entry corridor, and a significant fraction may be ejected back out into space on sub-orbital trajectories to collapse back on to the top of the atmosphere as seen with the Shoemaker-Levy 9 impact on Jupiter (Boslough and Crawford 1997).

3.1.3.3 Grain-size distribution Particles coarser than about 0.125 mm typically settle as individual fragments, whereas finer ash usually settles by clumping and falling as aggregates; hence the physics of tephra fall and removal differ for these two size classes, and they are represented differently in models. For volcanic eruptions, we have some sense of the fraction of erupted mass consisting of fine ash, and how it varies with eruption size, silica content, and the predominance of pyroclastic-flow activity in milling fine ash (Mastin et al. 2009; Rose and Durant 2009). For asteroid impact debris, we have little information to constrain this distal fine fraction. For the K-T impact event, Alvarez et al. (1980) assumed 22% based on nineteenth-century estimates from Krakatau (Symons 1888). Impact melt droplet size likely varies with impact size from micron-sized droplets seen in nuclear tests to hundreds of microns seen in the KT clay layer spherules (Melosh and Vickery 1991). Toon et al. (1997) estimate the lofted sub-micron unmelted dust as 0.1% of the mass of rock pulverized by the impact (100–1000× the meteor mass), again based on nuclear tests and the KT clay layer.

3.1.3.4 Wind field Simulations that forecast the path of an ash cloud during actual eruptions use wind fields taken from numerical weather prediction models (e.g., National Centers for Atmospheric Prediction, 2021). Historical eruptions are simulated using numerical wind fields (e.g., Kalnay et al. 1996) re-analyzed from historical meteorology. These wind fields typically extend only to about 30–40 km in the atmosphere. Debris from asteroid impacts may disperse from much higher elevation. To derive wind fields at such heights, meteorological models may have to be extended by incorporating empirical descriptions of the upper-atmosphere. This approach is currently used to develop a full atmospheric structure for tracking infrasound waves (e.g., Schwaiger et al. 2019).

3.1.4 Modeling the hazards

Several models are used regularly by volcano observatories during periods of unrest to assess volcanic hazards. The codes and their capabilities are listed in Table 2 for tephra dispersal, and Table 3 for debris flows. Ogburn et al. (2020) describes relevant codes to calculate volcanic ballistic ejection, and several other volcanic hazards. Explosive infrasound propagation (e.g., Schwaiger et al. 2019), shock waves (e.g., Dragoni and Santoro 2020), and climate effects (e.g., Schallock et al. 2021) are usually studied using codes tailored to that study.

Table 2 Models that simulate atmospheric transport and dispersal of tephra, smoke, and other particulates.

| Model | Configuration | | Output | | | References, comments, links | |
|----------|---------------|-----|--------|---|----|-----------------------------|--|
| | A | CA | D | A | DT | | G |
| Ash3d | E | W,C | x | x | x | x | Schwaiger et al. (2012); https://vsc-ash.wr.usgs.gov/ash3d-gui/#/ |
| Fall3d | E | O | x | x | x | x | Folch et al. (in review); http://datasim.ov.ingv.it/models/fall3d.html |
| Flexpart | L | O | x | x | x | x | https://www.flexpart.eu/ . Deposit arrival time is not calculated explicitly, but the deposit can be written out as a function of time. An example study that uses deposit output from Flexpart is Achterberg et al. (2013) |
| Hazmap | E | O | x | | | | Macedonio et al. (2005); http://datasim.ov.ingv.it/ . Hazmap can be run in two modes; one produces deposit maps from a single run, and the other executes many runs using a specified range of inputs and produces maps of exceedance probability of a given ash thickness |
| Hysplit | L | W,C | x | x | x | x | Stein et al. (2015); https://ready.arl.noaa.gov/HYSPLIT.php . Source code is available to registered users. Hysplit is generally used to model ash clouds rather than deposits, but one Hysplit variant is being used by the New Zealand Meteorological Service to model deposits (Hurst and Davis, 2017) |
| NAME | L | C | x | x | x | x | Jones et al. (2007); https://www.metoffice.gov.uk/research/approach/modelling-systems/dispersion-model . NAME has been used to simulate deposits at distal locations but is not regularly used to simulate proximal or medial tephra deposits |
| PUFFIN | L | OW | x | x | | x | Searcy et al. (1998); Bursik et al. (2013); https://vhub.org/resources/puffin/about |

For input, all models use a plume height, duration, grain-size distribution, and a description of the vertical distribution of mass in the initial plume. Some models may use a time series of these inputs. For input, the models also use a 3D, time-varying wind field, typically obtained from numerical weather prediction models or models that re-analyze historical meteorology, such as the National Oceanic and Atmospheric Administration (NOAA) NCEP Reanalysis 1 model (Kalnay et al. 1996). This list is not meant to be exhaustive

Configuration and capabilities: A = approach; Lagrangian (L), or Eulerian (E). In the Lagrangian approach, particles are inserted into the model and their movement is calculated through settling and advection. In Eulerian models, the atmosphere is divided into a 3D- grid and mass flux is calculated through cell walls as debris advects and settles. CA = code availability: open (O), web-accessible (W), controlled (C). Open-access models (O) are open source and available by download from the internet. Controlled-access models (C) are available by contacting the developer/research group to gain access

Outputs: D = map of deposit thickness or mass load; A = maps of airborne cloud properties; DT = deposit arrival time, fall duration at specified locations; G = grain-size distribution at deposit locations

Table 3 Models that simulate debris flow, which includes lahars. This list is not meant to be exhaustive

| Phenomenon | Model | Comments |
|--------------------------|--------|--|
| Debris flows | LAHARZ | Iverson et al. (1998); Schilling (2014). Open-source software that uses simple scaling relations between debris flow volume and planimetric area covered to delineate drainage areas likely inundated by debris flows or lahars. Inputs include lahar volume, and a digital elevation model of the drainage down which the lahar flows. Available at: https://pubs.usgs.gov/of/2014/1073/ |
| Landslides, debris flows | D-Claw | Iverson and George (2014); George and Iverson (2014). Open-source software (based on Clawpack) that solves differential equations for mass and momentum conservation of a depth-averaged granular-fluid mixture flowing over topography. Inputs include digital elevation models for topography as well as the geometry of an initial landslide mass. Additional inputs include material parameters for the landslide sediment and fluid mixture. Available at https://github.com/geoflows/D-claw |

3.2 Dust storms

Dust storms are a common hazard in many parts of the world, negatively impacting agriculture, infrastructure, transportation, human health, and quality of life. Because dust storms are more frequent over a larger portion of the globe than volcanic plumes, they provide another analog for downwind asteroid impact effects. If the impact location is near a large dust source (e.g., Bodélé Depression in Niger and Chad; Ravi et al. 2011), the high winds from the blast could mobilize a significant amount of dust, adding to the downwind hazard from the impact plume.

3.2.1 Application to planetary defense

The initial entry and impact of an asteroid will generate debris that will be lofted. This has already been discussed under volcanic plumes. In addition to creating suspended debris, the initial blast wave may also lift dust if appropriately sized sediment is available. The supply of dust that can be suspended will depend on location. The combination of impact-created debris and redistribution of previously deposited surface dust presents the possibility of future dust-lifting events (resuspension). The long-term impact of dust from an impact event will depend on both the composition and particle size and shape of the dust that is suspended or resuspended. While shelter-in-place orders may be issued

for the initial impact event for the areas where suspended dust will be an immediate hazard to humans and livestock, longer-term monitoring may be needed as resuspension may pose a periodic or episodic threat for years.

3.2.2 Current Knowledge and known effects

Dust storms can inject dust into the atmosphere that can be carried across continents, as well as transported to other continents. The large-scale transport of dust can have broad impacts to the atmosphere, by regulating solar radiation and cloud properties for example. Dust transport also impacts terrestrial and marine ecosystems over very large geographic extents. For example, dust from the African continent crosses the Atlantic Ocean and fertilizes the Caribbean Basin and the Amazon in South America (Prospero et al. 2021; Ravi et al. 2011, and references within).

However, smaller local and regional dust storms are also generally considered hazards with many negative effects, especially for agriculture, transportation, and human health, and can also affect infrastructure and industry as well as exacerbate drought conditions. For example, twentieth-century drought has turned the “Tigris” (Dicile) and “Euphrates” (Firat Nehri) basins that once formed the “Fertile Crescent” of “Mesopotamia” (Al Jazīrah) into the source of regional sand and dust storms that severely impact air quality and human health in the “Arabian Peninsula” (Shibh al Jazīrah al ‘Arabīyah) (Kelley et al. 2015; Notaro et al. 2015).

Human health is directly impacted through the inhalation of dust, especially when the mean dust diameter is 2.5 microns or less (PM_{2.5}). The health threat depends on dust quantity, particle size and composition, and whether the dust contains toxic fungal (e.g., *Coccidioidomycosis*) and (or) microbial components (Kellogg and Griffin, 2003). Dust is tracked by the Environmental Protection Agency (EPA). Dust can also increase the cost of water purification.

Agricultural impacts include both cropland and livestock. Long-term cropland productivity can be negatively impacted through erosion of topsoil. The deposition of dust, depending on composition, can degrade the quality of the soil. Short-term cropland productivity can be reduced from damage to the crops via “dust-blasting,” reduction of photosynthesis through the reduction of sunlight (Farmer 1993 and references within), or blockage of the stomata (Krajickova and Mejstrik 1984). Reduction in crop productivity due to dust storms has been observed but the size of the effect depends on many parameters, including crop type, dust particle size and composition, thickness of dust fallout, and season. The most direct effect of dust on livestock and humans is inhalation.

Transportation is negatively affected via two mechanisms: reduction in visibility and damage to infrastructure, vehicles, and equipment (e.g., Al Hemoud et al. 2019). Reduction in visibility along transportation corridors results in an increase in automobile accidents. Dust and sand deposition on roadways can create a situation requiring large costs for abatement and mitigation measures and for plowing and removal to keep corridors open for vehicles (e.g., Dong et al. 2002). Jet and internal combustion engines are damaged through the inhalation of dust, which result in engine failure due to increased friction and abrasiveness. Even without immediate engine failure, which increases the chances of loss-of-life for both air and ground transportation, the resulting damage will result in increased maintenance costs.

Dust transport and deposition exacerbate drought conditions if the dust is incorporated into the snowpack at higher elevations. The dust is darker than the snow and can result in increased absorption of insolation, resulting in early snowmelt (e.g., Painter et al. 2018).

3.2.3 Examples

3.2.3.1 American dust bowl of the 1930s An example of human activity exacerbating the effects of dust on a national scale is illustrated by the American Dust Bowl of the 1930s. Drought conditions were necessary but not sufficient to cause the dust bowl. Dry farming practices of the time disturbed the topsoil, making it more erodible and increasing dust emissions (e.g., Lee and Gill 2015). Perhaps the greatest lesson to be learned from the American Dust Bowl is more generalized than just drought and dust; it is that human activity and behavior can contribute and magnify the negative and costly effects of natural hazards. A firm understanding of the entire system which encompasses the natural disaster should be understood if mitigation efforts are to have their intended effects.

3.2.3.2 Iran A more recent (and ongoing) example of the effects and cost of dust storms on human civilization and health is Iran. Iran is 93.5% dryland desert (extra-arid, arid, or semi-arid; Rahimi et al., 2013) and has frequent, large dust storms that impact every aspect of life from infrastructure to health, physical and economic (Rashki et al. 2021, and references therein). Dust events have been linked to an increase in respiratory illnesses and lung cancer. Dust storms may also transport pollen, fungi, and heavy metals, which also result in respiratory illnesses. Heavy metals can have significant effects on the human cardiovascular system. In addition to health issues, dust storms in Iran reduce economic output. Abdolzadeh and Nikkhah (2019) found that solar energy can be reduced up to 16% annually due to dust deposition. High concentrations of dust can have detrimental impacts on crops, as demonstrated by Hatami et al. (2017, 2018) using field experiments on wheat and cowpea. Grapes (Behrouzi et al. 2019) and oak forests (Moradi et al. 2017) were also negatively impacted. The economic impact of reduced industrial productivity was estimated to be \$US 149 million (0.04% GDP) per day for large dust events (Birjandi-Feriz and Yousefi, 2017), mostly due to effects on workers' health and safety as well as disruptions in transportation. Meibodi et al. (2015) determined the total annual economic loss to Iran due to dust storms was \$US 1 trillion (1000 million).

3.2.3.3 Rural gravel roads Traffic on a rural gravel road is not usually considered a natural hazard. But on a small scale, this analog illustrates the effect of suspended dust on crops. McCrea (1984) conducted a study on the effects of dust on fruit crops where the dust was generated by traffic on rural unsealed gravel roads in northern New Zealand. While the methods employed were considered crude (as noted by the author himself), the results provide a rough order of magnitude estimate of crop loss due to road dust. Under nominal conditions, McCrea estimated that the productivity of affected acreage was reduced by 2–5%, depending on the fruit. While the affected acreage due to road dust is likely a small percentage of the total acreage in production (affected acreage is close to the road), one can imagine that a 2–5% loss in total crop production would have significant financial impact on farming where profit margins are typically tight.

Table 4 Models commonly used to characterize, predict, or track dust transport. This list is not meant to be exhaustive. <https://www.aarl.noaa.gov/hysplit/> as the URL for HYSPLIT

| Model name | Input | Output | Comments | References and URLs |
|---|--|---|---|---|
| Hybrid single particle Lagrangian integrated trajectory (HYSPLIT) | Location, Above Ground Levels (AGL), Time, for wind speeds extraction from atmospheric models or databases | The air-parcel path | Traces a parcel of air, but does not model fallout of suspended particulates Model can be run forward or backwards in time | HYSPLIT—2—Air resources laboratory (noaa.gov); NOAA's HYSPLIT transport and dispersion model; Dust—Air resources laboratory (noaa.gov) |
| Dust regional atmospheric modeling (DREAM) | Topography, vegetation cover and soil types; humidity, and wind patterns | Mean sea level pressure fields, 500 hPa geopotential height fields, Temperature fields and height profiles, wind speed height profiles, specific humidity height profiles, wind direction, PM2.5 and PM10 near ground layer dust concentrations and height profiles | Models dust cycle including lifting | Nickovic et al. 2001 Dust transport model validation using Satellite-and Ground-based Methods in the Southwestern United States.pdf (unm.edu); |
| Model for Atmospheric Transport & CHemistry (MATCH) | Meteorological data | Trace chemical and mineral transport distributions | | Rasch, P.J. Mahowald, N.W., and Eaton, B.E. 1997. Representations of transport, convection, and the hydrologic cycle in chemical transport models: Implications for the modeling of short-lived and soluble species. <i>Geophys. Res. Lett.</i> 24, 28, 127–130 |
| Community Atmosphere Model (CAM) | Requirements for input dataset are found in the Users' Guide | General meteorological data | Earlier versions were called Community Climate Model (CCM) | Users' guide: https://www.cesm.ucar.edu/models/cesm1.0/cam/docs/ug5_1/ug.html |

Table 4 (continued)

| Model name | Input | Output | Comments | References and URLs |
|---|--|--------------------------------------|--|---|
| Mineral Dust Entrainment and Deposition (DEAD) | Wind speed profiles, vegetation cover, and surface soil moisture Inputs may be provided through MATCH or CCM | Wet and dry deposition distributions | Models dust cycle including lifting. DEAD can be implemented as a component of MATCH | Zender, et al. (2003) Mineral Dust Entrainment and Deposition (DEAD) model: Description and 1990s dust climatology—Zender—2003—Journal of Geophysical Research: Atmospheres—Wiley Online Library, and references within |
| Community Aerosol and Radiation Model for Atmospheres (CARMA) | For dust storm forecasting, inputs include winds, pressure, and temperature at the surface and at multiple pressure levels | Dust concentration maps | Dust Transport Model, but also includes a radiative transfer component | Toon et al. (1988); Ackerman et al. (1995); Barnum et al. 2004. Source code: https://github.com/ESCOMP/CARMA |

3.2.4 State-of-the-art models

Dust storm models, such as HySPLIT, can be used to trace where dust goes once suspended, but do not predict specific dust-lifting events. Other models, such as Mineral Dust Entrainment and Deposition (DEAD), include both the prediction (or parameterization) of dust-lifting events and downwind dust dispersion. HySPLIT could be useful to track low-altitude fine-grain ejecta, but adjusted winds would be needed as the standard wind input would not include the winds created by the overpressure. If an asteroid impact occurred in a dusty region, models such as DEAD could be used to estimate the additional dust that could be lifted, but once again, the wind regime for the model would need to be adjusted to account for the overpressure. Models such as DEAD would be useful to estimate longer-term resuspension events that could be problematic for years (Table 4).

3.3 Wildfires—smoke, post-fire flooding, erosion and sedimentation as analogs

As an analog for an asteroid impact, there are two types of wildfire hazards that are relevant: (1) the initial smoke and ash that is transported by the winds and (2) the surface aftermath of the fire. Smoke is discussed in Sect. 3.3.1. The remaining sections discuss the cascading hazards that occur because wildfires alter both vegetation cover and soil properties. When fires burn vegetation and the soil surface, it reduces the protective cover of those elements, permitting fluids (water or air) to flow faster across the land surface and impart greater erosive force on the soil surface (Fig. 3)

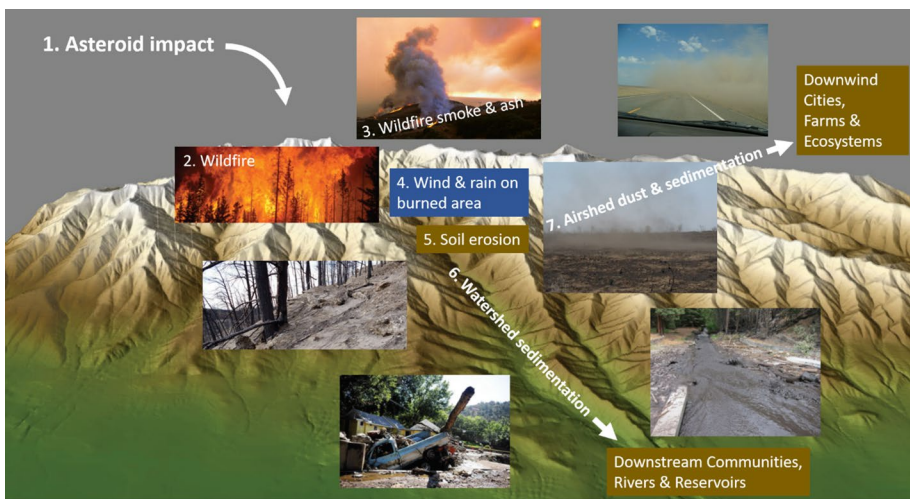


Fig. 3 Wildfire initial effects and cascading hazards. Figure Credit: A. Kasprak and J. Sankey; Photo Credits: U.S. Geological Survey Multi-Media Galleries, USDA Forest Service, and J. Sankey

3.3.1 Wildfires—smoke

Smoke from wildfires is often thought of as a local effect. While this may be true for smaller isolated wildfires, it has become obvious that wildfire smoke from larger wildfires can be regional. For extremely strong wildfires, the smoke can enter the troposphere and be transported across continents and oceans (e.g., Baars et al. 2021). With the increase in both number and intensity of wildfires, smoke is affecting increasingly larger areas that are downwind. The High-Resolution Rapid Refresh-Smoke forecast model is a new experimental method of tracking and forecasting smoke height. (Benjamin et al. 2016). According to NOAA, "It is the first weather forecast model in the U.S. to include smoke's impact on weather, and it has become a vital resource for fire crews, air traffic controllers, local forecasters, and even school administrators." (NESDIS, 2021) The Environmental Protection Agency (EPA) tracks the wildfire smoke as a human health hazard (e.g., Wildfires and Indoor Air Quality (IAQ)|US EPA). Fire air pollution—in the form of particulate matter (PM₁₀), fine particulate matter (PM_{2.5}), and ozone (O₃) pollution—is harmful for human health (Anenberg et al., 2010; Lelieveld et al., 2015; Pope et al., 2009; Reid et al., 2019) and costly economically (Fann et al., 2017; Rappold et al., 2014; Rittmaster et al., 2006), but its effect on ecosystems is uncertain.

3.3.2 Post-fire wind erosion and dust emissions

Aeolian sediment transport is a function of the wind's ability—impeded by vegetation and terrain—to entrain soil particles, and the soil's susceptibility to this entrainment (Bagnold, 1941, Okin et al., 2006). Increased wind erosion of soil has been reported immediately following fires in a wide variety of landscapes across the world, including shrublands and forests (Whicker et al. 2002, Zobeck et al. 1989, Sankey et al. 2009, 2010; Dukes et al. 2018), grasslands (Vermeire et al. 2005; Ravia et al. 2009), and desert dune fields (Thomas and Leason, (2005), Wiggs et al. (1994), Wiggs et al. (1995), Wiggs et al. (1996)). Specifically aeolian sediment flux via saltation and dust emission has been reported to increase by up to several orders of magnitude for weeks to years following fire (see reviews in Sankey et al. 2009; Miller et al., 2012). Wind erodes carbon (Hasselquist 2011), biologically important nutrients, (Sankey et al. 2012; Wang et al. 2019), pollutants, and contaminants (Whicker et al. 2006) from burned areas and deposit them in downwind environments. Dust emitted from burned areas can negatively impact air quality in downwind human communities (Hahnenberger and Nicoll 2012; Hahnenberger and Nicoll 2014).

3.3.3 Post-fire flooding

Flooding is common after wildfires. Wildfires can decrease soil infiltration rates (McGuire et al. 2018; Nyman et al. 2014; Onda et al. 2008), decrease soil structure and organic matter content (Chapin III et al. 2002), and increase soil erodibility (Moody et al. 2005). Runoff is often generated following wildfire when rainfall exceeds the infiltration capacity of the soil and thus runs off the ground surface downslope (termed infiltration-excess overland flow) due to reductions in canopy storage capacity, removal of litter and duff layers, and changes in soil hydraulic properties that reduce infiltration capacity (e.g., Moody and Ebel 2014; Schmidt et al. 2011; Ebel 2020). As a result, even short-duration rainstorms with frequent recurrence intervals may have sufficient rainfall intensities to exceed the infiltration capacity (Staley et al. 2020).

3.3.4 Post-fire rainfall-runoff soil erosion

Burned areas within watersheds cause water to runoff faster and in larger volumes after rainstorms, and also make soil erode faster and in larger volumes due to rainfall and runoff (Shakesby and Doerr 2006; Shakesby 2011; Moody and Martin 2009; Miller et al. 2011; Pierce et al. 2004). Sediment that erodes from hillslopes can ultimately end up in channels, streams, and reservoirs faster and in larger volumes than would otherwise occur without fire (Weidner and Todd 2011; Murphy et al. 2015; Smith et al. 2011). Increased sediment can dramatically—often negatively—impact aquatic ecosystems, decrease water quality and supply, and increase the cost of water delivery to people (Shakesby and Doerr 2006; Palmieri et al. 2001; Smith et al. 2011).

Changes that fire imparts on the land surface in watersheds include the losses of plant canopy, ground cover, and soil organic matter, as well as enhanced soil water repellency (DeBano 2000; Certini 2005). Losses of plant canopy and ground cover reduce interception of rainfall and transpiration. Loss of ground cover reduces soil surface roughness and increases the velocity of fluid flow across the landscape. Loss of ground cover increases the potential for soil surface sealing. Loss of ground cover and soil organic matter can increase rainsplash effects and soil erodibility in general. These factors individually and collectively lead to increased runoff in the form of base flows, peak flows and water yield from watershed hillslopes and channels, and lead to increased soil erosion via rainsplash, sheetwash, rilling, gully and mass-wasting processes.

Wildfire heats the near-soil surface and propagates a high temperature creating a strong thermal gradient. The heat flux is governed by the ability of the fire to evaporate water in soil pores (Campbell et al. 1995). The depth of heating is often shallow, on the order of 5–10 cm (Rengers et al. 2017), but in locations with large amounts of fuel smoldering can propagate a heat pulse up to 1 m (Massman et al. 2003). Heating increases soil erodibility by killing fine roots (Nyman et al. 2013a, b), destroying plant tissue, roots, and soil microorganisms, which all play a part in soil cohesion and structure (Hungerford et al. 1991; Busse et al. 2010; Chief et al. 2012). Expansive 2:1 clays are destroyed or altered during wildfires (Fitzpatrick 1980; Chandler et al. 1983; Ulery et al. 1996; Arocena and Opio 2003), thus further reducing soil cohesion. Consequently, wildfire reduces overall soil cohesion and structure, which makes it easier to erode soils after wildfires.

3.3.5 Post-fire mass wasting: debris flows and landslides

Wildfires increase the likelihood of several forms of mass wasting (e.g., debris flows, landslides, rockfalls) by influencing the hydrology, soils, and vegetation in steep forested settings (e.g., Santi and Rengers 2020). For the first 1–3 years after a wildfire, there is an elevated risk of runoff-generated debris flows on steep slopes (>23 degrees) in burned areas (e.g., Staley et al. 2017). Debris flows are mixtures of both sediment and water, but the depth and discharge of debris flows are many times greater than water flows (Kean et al. 2016). When rain falls on burned slopes, infiltration rates are typically lower than unburned soils due to enhanced hydrophobic conditions (DeBano 2000; DeBano et al. 1979), hyper-dry conditions (Moody and Ebel 2012), or surface soil sealing (Larsen et al. 2009). This results in increased water runoff, which is further enhanced by a lack of water storage in burned forests (Larsen et al. 2009; Parise and Cannon 2012) due to ground cover reduction and a lower hillslope roughness (Cerdà and Doerr 2005; Liu et al. 2022; Noske et al. 2016). Consequently, when water runs off quickly, it can transport burned soil and

rock, and the water-dominated flow can transition to a debris flow through either progressive entrainment of material or en-masse failure in channel beds (McGuire et al. 2017). As can occur with post-fire rainfall-runoff soil erosion, debris flows can also move fine sediment into municipal water supply reservoirs, which decreases the water quality (Langhans et al. 2016).

Although the threat of runoff-generated debris flows wanes several years following fire, the likelihood of shallow-landslides can increase. As the threat wanes, watershed soils recover pre-fire infiltration rates and vegetation regrows, both of which reduce the overland flow that is prevalent immediately following a wildfire (Liu et al. 2021). However, roots of large plants prior to the fire continue to decay for several years after a wildfire, and this can reduce root-reinforcement on steep, burned slopes (Jackson and Roering 2009). Root-decay coincides with the increase in soil infiltration rates, making steep slopes particularly susceptible to landslides several years after a wildfire (e.g., Rengers et al. 2020). Consequently, the hazard of post-fire mass movement begins with a threat of runoff-generated debris flows but can transition to a threat of post-fire landslides. This can extend the likelihood of mass wasting for a decade or more, after the initial wildfire.

3.3.6 State-of-the-art models

A variety of hydrologic modeling approaches have been used to estimate post-wildfire hydrology (e.g., Nyman et al. 2013a; Kinoshita et al. 2014; Ebel et al. 2020). All the models simulate an increase in runoff that is due to a combination of reduced soil water infiltration, a reduction in water storage due to burned surface litter/duff, and an overall reduction in roughness from vegetation incineration. Relatively simple non-distributed modeling methods are frequently applied for timeliness (e.g., USDA TR-55 (USDA 2009), Wildcat-5 (Hawkins and Munoz 2011), U.S. Geological Survey Linear Regression Equations (see Kinoshita et al. 2014), Rowe, Countryman, and Storey (1949), and Wilder et al. (2021)). Distributed models such as HEC-HMS (USACE 2010) and Kinos2 (Goodrich et al. 2012) are used more frequently to estimate distributed rainfall and runoff. Recently, more sophisticated models have been introduced to incorporate 3D-soil water-infiltration effects (e.g., InHM of VanderKwaak 1999; in Ebel et al. 2016) and to allow for flow routing over detailed lidar-derived topography (e.g., Rengers et al. 2016).

A suite of applications developed from the Water Erosion Prediction Project (WEPP) (Elliot et al. 2006) are commonly applied models for post-fire rainfall-runoff soil erosion processes on burned national forests and other public lands in the USA (see Forest Service WEPP Interfaces; <https://forest.moscowfsl.wsu.edu/fswcpp/>; Miller et al. 2011; Sankey et al. 2017). WEPP is a process-based model that uses inputs from topography, vegetation, soils, and land management. A spatially distributed, physically based hydrological model routes water and sediment across hillslopes and small watersheds up to the scale of several square kilometers ($\sim 5 \text{ km}^2$) and is driven by daily weather data that can be either created from historical measurements or generated from a stochastic weather generator, Cligen, which generates WEPP climate inputs from a database of thousands of weather stations within the USA (Flanagan and Nearing 1995). WEPP uses the climate data to model runoff, erosion, and sediment delivery by event, month, year, or average annual values for time periods ranging from one storm to one millennium for either an individual hillslope or a watershed containing many hillslopes, channels, and impoundments (Flanagan and Nearing 1995; Larsen and MacDonald 2007). WEPP calculates inter-rill (e.g., sheetwash) erosion, rill erosion, and erosion in small channels (i.e., ephemeral gullies) in areas of flow

Table 5 List of example models used to estimate cascading effects from wildfires caused by hydrological and erosional processes. This list is not meant to be exhaustive. <https://data.nal.usda.gov/dataset/small-watershed-hydrology-wintr-55> as the URL for TR-55, <https://www.slf.ch/en/services-and-products/ramms-rapid-mass-movement-simulation.html> as the URL for RAMMS, <https://flo-2d.com/product/mud-and-debris-flow-training-package/> as URL for Flow-2D

| Model | Application | References or URLs |
|----------------------------------|--|---|
| USDA TR-55 | Runoff and hillslope hydrological processes | WinTR-55 watershed hydrology NRCS (usda.gov) |
| Wildcat-5 | Runoff and hillslope hydrological processes | Hawkins and Munoz 2011 |
| USGS Linear Regression Equations | Runoff and hillslope hydrological processes | Kinoshita et al. 2014 |
| HEC-HMS | Distributed rainfall and runoff hillslope hydrological processes | USACE, 2010 |
| Kineros2 | Distributed rainfall and runoff hillslope hydrological processes | Goodrich et al. 2012 |
| WEPP | Rainfall-runoff soil erosion processes | https://forest.moscowfsi.wsu.edu/fswepp/ |
| D-Claw | Debris flow processes | George and Iverson 2014; Iverson and George 2014 |
| RAAMS | Debris flow processes | RAMMS—Rapid mass movement simulation—SLF |
| Flo-2D | Debris flow processes | Mud and debris flow—FLO-2D software |

convergence. The WEPP model does not include landslides, channel erosion, or debris flows. The Forest Service WEPP Interfaces currently include WEPP applications for spatially explicit modelling of soil erosion and sediment yields following fire disturbance (Larsen and MacDonald 2007; Elliot et al. 2006) in the USA, Europe and Australia using geospatial topography and soils data and local climate.

Debris flow modeling is complex because it requires water-flow routing as well as the interaction between fluid and granular material. The physics of debris flows can be modeled well using the D-Claw model (George and Iverson 2014; Iverson and George 2014) or sediment transport models that explicitly account for debris flow physics (e.g., McGuire et al. 2016). Reduced complexity models can also be used to simulate debris flow peak timing and locations of debris flow initiation (Rengers et al. 2016, 2019) while maintaining fewer model parameters requiring calibration. Debris flow inundation can be estimated using models such as D-Claw, RAAMS, and Flo-2D (Barnhart et al. 2021). Debris flow inundation modeling primarily relies on accurate estimates of the initial debris flow volume (Barnhart et al., in review). Empirical models designed to estimate debris flow volume are tied to the local topography, climate, and tectonic history of the mountain ranges in which they were developed (Rengers et al. 2021). Consequently, a global model for debris flow volume has not yet been developed (Table 5).

3.4 Earthquakes

Earthquakes caused by tectonic motion can be used as analogs for seismic waves from asteroid impacts. Some care must be taken with the initial effects as described below, but the long-term cascading hazards from debris, landslides, and other effects will be the same regardless of the source of the seismic waves.

3.4.1 Tectonic versus impact seismic waves

The largest recorded tectonic earthquake was magnitude 9.5 in Chile in 1960, releasing about 10^{19} Joules (2.4 Gt) of seismic energy. Only about 1–10% of the energy goes into seismic waves depending on the stress drop and properties of the local rock, with most of the energy going into fracture or frictional heating (Bormann et al. 2013). Earthquake recurrence generally follows a power-law distribution with magnitude with about 100,000 earthquakes per year greater than magnitude 3, which is about the limit of human perception, but only a few events per year $M > 8$ capable of causing widespread damage, only a few per century $M > 9$, and there is no tectonic plate on Earth large enough to have a fault that could realistically create a magnitude 10 earthquake.

Volcanic eruptions can also cause earthquakes and are generally less efficient at producing seismic waves than tectonic slips but can reach magnitude 6. Well-confined, buried chemical or nuclear explosions can achieve efficiencies of up to 0.1% (Bormann et al. 2013). For asteroid impacts efficiencies are 0.1% at the high end but can be as low as 0.001% (Collins 2005; Robertson 2017). Using an efficiency of 0.01%, a 125-m-diameter asteroid impacting the ground with 125 Mt energy will create a magnitude 6 earthquake, and a 1-km-diameter (50,000 Mt) asteroid will create a magnitude 7.7 earthquake, and a 12-km-diameter (115 million Mt) asteroid would create a magnitude 10 earthquake (Toon et al. 1997).

Explosions and impacts are less efficient at creating seismic waves because a strike-slip earthquake produces a quadrupole source with more energy being transferred into shear waves, whereas explosions provide a monopole source with more energy transferred into pressure waves. (Bormann et al. 2013). Pressure and shear waves expand spherically as the reciprocal distance squared ($1/r^2$) from the epicenter but can be trapped at the surface and become surface waves (Rayleigh and Love waves). At distances of interest (significant but not devastating damage), the peak velocity or acceleration decays as roughly $1/r$ due to geometric spreading of the surface waves (Wald et al. 1999; Atkinson and Wald 2007). Vertical oscillations are the most damaging, which the Rayleigh waves provide, and strike-slip earthquakes efficiently create. For an impact the vertical motion is not efficiently generated by the shock (pressure) wave propagating out from the impact. The Rayleigh waves (gravity waves like ripples on a pond) can, however, be generated by the pressure wave reflecting off the Mohorovicic discontinuity (the Moho) which will send pressure waves back to the surface with a vertical component, and also by rebound of pulverized rock in the crater.

Damage due to seismic waves is tightly correlated with vertical peak ground acceleration or velocity. If peak ground acceleration exceeds 9.8 m/s^2 (1 g), objects are thrown into the air and most buildings will collapse. Once acceleration drops below about 5% of g, the damage is negligible. Buildings are particularly sensitive to vibrations around $1 \text{ Hz} \pm$ a factor of 10, so some intensity estimates include spectral filtering of seismometer measurements (Shabestari and Yamazaki 2001). Impacts are typically of short duration (~seconds), so they excite more high-frequency oscillations than tectonic earthquakes, which can last up to minutes.

3.4.2 Initial and cascading effects

The fatality rate depends on the intensity and the local quality of construction. In affluent earthquake-prone regions with strict construction codes, such as California, most buildings are designed to survive up to an earthquake intensity Modified Mercalli Intensity (MMI) 10 ($> 1 \text{ g}$ acceleration) and the expected fatality rate is only 1 in 10,000. Conversely at MMI 10, the expected fatalities in poorer regions with weak construction may exceed 1 in 10. For California, the expected fatality rate drops below 1 in a million for MMI 7 ($\approx 1/4 \text{ g}$) and for the most vulnerable places at MMI 5 ($< 10\% \text{ g}$), which would mostly break a few windows and dishes in a typical house (Jaiswal et al. 2009).

While the damage caused by an impact-induced earthquake may be largely restricted to the areas more greatly damaged by the later arriving blast wave, its effects should not be underestimated as the earthquake damage could set the stage for a cascade of additional natural disasters that could cause havoc on decadal timescales as shown by the 1999 Jiji, Taiwan and 2008 Wenchuan, China earthquakes (Fan et al. 2018) and the 2016 Kaikoura, New Zealand earthquake (Massey et al. 2018). Particularly in urban areas, collapse of power lines and breaking of power cables can start fires, which can result in toxic emissions from chemical fires (Moussa and Devarakonda 2014; Celano and Dolšek 2021). Even outside of urban areas, the M6.7 1927 “Crimean” (Krym) earthquake released methane, hydrogen sulfide (H_2S), and phosphine from the seabed of the “Black Sea” (Prychornomors’ka Nyzovyna) which spontaneously ignited, resulting in many fires as well as the release of toxic gases (Schuiling et al. 2007).

The large amount of debris generated can be washed into rivers by rains. In particular for urban areas, this can include many toxic household materials such as gasoline, oil,

tar, bleach/cleaning chemicals, paint, and batteries, (Reinhart and McCreanor 1999) as well as toxic chemicals from industrial facilities such as the 6500 tons of acrylonitrile released from ruptured storage tanks after the M7.6 İzmit, Turkey earthquake (Steinberg and Cruz 2004). Five years after the M6.8 2003 Boumerdes, Algeria earthquake, heavy metal content in wells near the landfill site where debris was disposed was 5 times the national limit showing leachate had reached the aquifer (Benmenni and Benrachedi 2010).

Earthquakes can also induce damage at extended distances. Landslides into water and underwater landslides can also cause tsunamis. Indeed, the majority of landslide tsunamis are thought to have been caused by earthquakes. The hazard depends greatly on the location and size of the landslide (Ten Brink et al. 2010; Løvholt et al. 2008, 2015).

Landslides can cause chain reactions of hazards of debris flows, landslide dams, dam-break floods, sediment/debris transport, and riverbed uplift that can play out over decades. Many earthquakes in mountainous areas trigger landslides. China's M7.9 2008 Wenchuan earthquake created an estimated 10^{10} m³ of total landslide volume of which 15–20% created over 800 landslide dams. The dams created a storage capacity of about 10^9 m³ and 25% failed within a week, but ~10% were still intact after a year. (Fan et al. 2012). In the immediate aftermath of the earthquake, 25% of the almost 80,000 missing or dead were due to landslides. In the town of Beichuan, the earthquake collapsed 80% of buildings in town and, together with 2 induced landslides, killed 2300 people. In the 5 years after the earthquake, the town suffered 6 more disasters leading to the loss of 6700 more people: A month after the earthquake, a landslide dam upstream was breached and a flood swept through town. In the fall, a storm swept loose landslide deposits into town burying most of the old town. This, in turn, caused the river to change course scouring part of the town. Over the next 5 years, the riverbed in town rose 15–38 m due to excessive sedimentation brought from landslides upstream. Finally, due to the elevated riverbed, a storm caused the river to overflow and flooded 80% of the town (Zhang et al. 2014).

A similar story was created by the M7.8 2016 Kaikoura earthquake, which created > 196 landslide dams that temporarily blocked rivers (Massey et al. 2018; Jibson et al. 2017). The dams reached sizes ranging from 100–1000 million cubic meters, creating hazards for downstream infrastructure and life (Jibson et al. 2017). The largest example was a dam on the Hapuku River that was 100 m high, which was breached five months later by Cyclone Cook and produced several debris flows (Massey et al. 2018).

3.4.3 ShakeMap

ShapeMap software was developed by the US Geological Survey (USGS) Earthquake Hazards Program (Wald et al. 1999, 2009; Worden et al. 2010). ShapeMap can be used to generate maps of peak ground motion for either real events or for use in emergency management exercise. ShapeMap can be downloaded at <https://earthquake.usgs.gov/data/shake-map/>.

3.5 Hurricanes and Tornadoes

Hurricanes and tornadoes provide a useful analog to blast winds at large distances from a large impact. Data on large blast waves from nuclear explosions generally stop around 1 psi overpressure where most buildings can survive the blast and the fatality rate drops

below ~1 in 100 (Glasstone and Dolan 1977). For hurricanes, damage is well recorded to much lower windspeeds than for blasts and, in the USA, people evacuate hurricanes to the 1 in a million-fatality risk, (Lindell et al. 2006).

In hurricane- and tornado-prone areas in the USA, adherence to building code requirements means that most houses can withstand most winds they are likely to experience over a 50-year period. Consequently, most of the damage is either from uncommon category 5 winds or is due to buildings not designed to withstand the winds, such as mobile/pre-fabricated homes, garages, sheds, and also buildings in storm surge flood areas (Lindell et al. 2006).

For Chelyabinsk (Popova et al. 2013), the blast wind behind the ~0.5 psi shock wave and the 2 nearly fatal injuries and 1500 hospitalizations out of a population of 1.1 million, both roughly match the expected windspeed and casualties if a tropical storm had hit instead of a meteor.

Long-term hurricane effects are mostly related to pollution from toxic debris. Debris clean-up accounts for up to 40% of disaster-related costs (EPA 2019). Most debris and pollution come from two sources: wind and flood. For hurricanes, associated heavy rains wash pollutants into streams and the ocean and, for the most polluting hurricanes, the majority has come from mobilizing chemicals, fuel, sewage by flooding (Han et al. 2022; Sheikh 2005). For a land impact of an asteroid, the flooding and rains will be absent, allowing more time for clean-up before pollutants leach into the soil. Tornado clean-up may be a better analog.

A typical hurricane produces ~10 times the normal annual waste in a single event (Reinhart 1999). As an example, in 2004, Hurricanes Charley, Frances, Ivan, and Jeanne hit in short succession causing 47 deaths, \$45B in damages, and the displacement of 1.7 M people. Local contractors cleared >4 M cubic meters of debris. Eighty percent was vegetative (e.g., downed trees), and 20% comingled (e.g., buildings). More than 3 M cubic yards of the vegetative debris was chipped into mulch. After Hurricane Ivan, the vegetative debris was disposed of with 60% going to a biomass power plant for energy generation, 15% was sent to paper mills, 15% used for landfill cover, and 10% incinerated (EPA 2019).

Following Hurricane Katrina for example, household hazardous waste was segregated curbside, so most batteries, propane cylinders, gasoline, oil, ammunition, electronics, and refrigerators were recycled. Seafood from the fishing industry in Gulfport, Mississippi, was of particular concern but disposed of quickly before it spoiled to prevent it becoming a health hazard. However, the hurricane resulted in >100 M m³ debris, exceeding the capacity of existing disaster debris plans and infrastructure. Insufficient waste processing sites, and lack of impermeable liners at improvised waste management sites lead to problems with pollutants. Drywall produced H₂S gas, and arsenic from pressure-treated wood (construction) leached into groundwater. Vegetative debris was infested by termites so was quarantined, limiting disposal options (EPA 2019).

4 Discussion

Under ideal conditions, humanity would discover a hazardous asteroid that is on an intercept course with the Earth decades in advance, allowing for the deliberate development of mitigation (deflection or catastrophic disruption) missions. However, this may not be the case and the warning time may not be sufficient for asteroid mitigation missions to be launched. Under this scenario, civil defense mitigation strategies will be needed. Current

modeling efforts that predict initial effects from a meteor impact or airburst provide needed information for initial preparation and evacuation plans, but longer-term cascading hazards are not yet characterized. More common natural disasters are analogs to provide scope and scale of potential effects. These events, especially the larger events with cascading effects, are key for understanding the scope and complexity of mitigation, relief, and recovery efforts.

4.1 Cascading hazards

The detrimental effects of a medium-sized asteroid impact could last for years. Examples of the complexity and time span of cascading hazards are the Mount Pinatubo eruption and the 2008 Wenchuan Earthquake. The impact of cascading hazards lasted for years, extending into what would usually be considered the recovery phase of a natural hazard. The traditional phases of mitigation, relief, and recovery may need to be refined for a medium-sized impact event, or at least, planning considerations should recognize that these phases may have significant overlap or may be discontinuous (e.g., the mitigation phase may become an annual event if the cascading hazards are triggered by annual monsoons or snowmelt).

Cascading effects are not restricted to the area that was initially impacted or evacuated. The larger area of potential future hazards should be prominent in emergency and recovery plans. For example, evacuation destinations should be well outside the areas of potential cascading hazards. Recovery plans should consider mitigation efforts beyond the area of original damage. For example, flood control measures may need to be implemented hundreds of kilometers downstream from the affected watershed(s).

Finally, the magnitude, distribution, duration and damage caused by regional and (or) cascading effects will depend on location and season of the asteroid impact event. Initial downwind effects will depend on the prevailing winds at the time of impact and the use of the lands downwind at the time of impact. Because wind profiles are variable, predictions of possible damage will need to be probabilistic. Downstream effects are typically triggered by extreme precipitation. While precipitation events are usually seasonal, the amount and duration of each individual event can vary from storm-to-storm and season-to-season. As with the downstream damage predictions, the downstream damage predictions will also need to be probabilistic.

4.2 Evacuations and disaster diaspora

Hurricanes are not necessarily a good analog for the physical effects (except for high winds) of an asteroid impact, but may represent the complexity of conducting large-area evacuations. The population with the ability and the resources to self-evacuate will do so, but the timing of self-evacuation needs to be tightly controlled to prevent transportation corridors from becoming clogged. The population without the ability to self-evacuate becomes a problem of both the coordination of transportation assets and the identification of locations that have appropriate facilities to care and house the evacuees. It should be noted that many of the evacuees will never return home and will need long-term housing and employment. The region surrounding the initially damaged zone must also be considered in the recovery efforts. The areas, especially with high levels of poverty, may not be able to sustain even poverty-level quality of life post-impact if the area continues to be

affected by cascading events. The aftermath of Matthew (October 8, 2016) and Florence (September 14, 2018) in Robeson County, North Carolina, provides an historical example (Marson and Legerton 2021).

Human response and behavior add an additional dimension. Some fraction of the population will insist they be allowed to ride out the storm. This may be based on previous experience where they have survived previous events without evacuation. Unlike hurricanes, which occur on a regular basis along much of the coastal regions and therefore is a common experience that the community can intrinsically understand, a medium-sized asteroid impact event ranges from approximately one in a 100,000-year event ($\sim \varnothing 300\text{m}$) to a one in a million-year event ($\sim \varnothing 1\text{km}$). By comparison, the probability of a large volcanic eruption ($\geq \text{M}8$) in the next one-million years is 75% (Mason et al. 2004). In addition, an asteroid impact event of this magnitude would likely be known years in advance, providing civilization time to either act, react, or ignore. While this review paper has focused on geophysical and atmospheric hazards, the COVID-19 pandemic provides an example of human behavior that can complicate mitigation and evacuation efforts (Rocha et al. 2021; Stanley et al. 2021). Undoubtedly, there will be a fraction of the population that will call the warning of imminent impact a hoax. This is just one example of human behavior that must be considered during the planning process.

4.3 Climate change

Climate change will inevitably add complexity to the cascading effects from a medium-sized asteroid impact. Periods of extended drought and (or) extreme weather are likely to enhance the probability and intensity of potential cascading hazards.

Extended drought conditions stress ecosystems and reduce natural resiliency. The short-term and long-term hazards from an impact event may be more severe due to these stressed conditions than would have otherwise occurred. For example, wildfires may be more extensive that would otherwise be expected. Additional debris, especially organic debris, may be generated and could later be washed into streams and rivers.

Many of the cascading hazards discussed in this review center around external triggers, such as intense rainfall, resulting in a chain of events that lead to downstream flooding. Because cascading hazard mitigation may last for years or even decades, recovery efforts should consider the potential for changing climate scenarios on the same timescale.

4.4 Integrated framework: modeling, monitoring, and mitigation

A framework is needed for the modeling, monitoring, and mitigation of asteroid impact or airburst events, and the subsequent cascading hazards that result. This approach is not new as it was promoted two decades ago. “The principles of adaptive planning in the face of uncertainty fundamentally affect mitigation investment decisions. Civil defense measures have the advantage that improvements can be gained due to synergism with more mundane natural hazards.” (Morrison et al. 2002, p.750). In 2017, the US Geological Survey identified the need for, and the potential of, an integrated system that could be used to monitor, characterize, and forecast the increasing number and intensity of extreme climate events and identify the increased stress on both human and ecosystem resiliency (Jenni et al. 2017).

Ideally, this would be an integrated system that uses both state-of-the-art knowledge and models to provide the best actionable information to all stakeholders. Continuous state-of-the-art monitoring would either be used to validate or update predictions. Mitigation (including recovery) efforts would be conducted in accordance with the state-of-the-art actionable information, considering that cascading effects can and will be displaced in both time and space.

4.4.1 Modeling

Ideally, a comprehensive multi-hazard model could be developed, providing timely actionable information to all appropriate stakeholders. Current multi-hazard models are in their infancy and are tailored for a specific event. Substantial incremental progress could be made by coupling currently available hazard models, where the output of one model becomes the input of the next model. This approach can be cumbersome if the interface between models is manual transcription. Another complicating factor is that the model output may not span all the next input model parameters, necessitating the use of assumptions. Weather must also be considered in linking together cascading hazard models as precipitation is often the trigger to initiate the next event. A probabilistic approach will likely be needed as weather patterns have large uncertainties. This requires individual models to execute quickly so that an ensemble of possible outcomes can be compiled.

4.4.2 Monitoring

Monitoring would likely have three phases: (1) pre-impact event characterization, (2) monitoring of initial impact effects, and (3) long-term monitoring to ensure actionable knowledge remains current, accurate, and viable.

Pre-impact event characterization ensures hazard model inputs are current and state of the art. This characterization provides a foundational geospatial dataset for comparison to post-impact conditions. Monitoring of initial impact effects should include areas surrounding the expected damage area, especially the areas downwind. For example, differences in expected atmospheric dust loading may result in changes in no-fly zones in real-time. Long-term monitoring data can be assimilated into the multi-hazard models, providing updates to actionable information for all stakeholders. Monitoring efforts should include air quality, water quantity and quality, dust distribution, status of crops, and changes in local topography—especially in watersheds.

4.4.3 Mitigation

Current asteroid impact hazard models provide actionable intelligence for levels of evacuation in the immediate damage area. But outside this immediate area, additional short-term mitigation may be needed, such as closing both air and ground transportation corridors (due to suspended fine particle debris) and extending air quality warnings and alerts for both humans and livestock. Depending on the season and location of the impact, farmers in downwind areas may be instructed to fallow their fields prior to impact to minimize the economic impact of crop destruction.

Long-term recovery efforts may need to include long-term mitigation strategies for cascading hazards. These mitigation strategies and plans should consider a much larger area than the initial impacted area, due to cascading hazards that could last for years and extend

both downwind and downstream from the initial impact damage zone. Mitigation strategies should identify potential external triggers, such as extreme rain, that could initiate a cascading event (e.g., Zhu et al. 2021). A combination of monitoring and modeling could be used to predict future hazards, as demonstrated by Zhang and Matsushima (2018) for debris flows.

4.4.4 Metrics and vulnerability estimates

This paper has mainly focused on the cascading effects from natural hazards. We have alluded to the vulnerabilities of society to these effects, such as a decrease in crop production (e.g., Sect. 3.1.1), loss of economic output (3.2.3), or even loss of life (Sect. 3.4.2). While beyond the scope of this paper, vulnerability modeling is needed to convert cascading effects described in this paper into quantifiable cost (or metric). Examples of this have been conducted for initial effects of an asteroid impact (e.g., Mathias et al. 2017; Rumpf et al. 2017). Metrics used in these vulnerability studies have included estimated fatalities (e.g., Rumpf et al. 2017), affected population (Mathias et al. 2017), or total monetary cost of damages. Because warning times should be sufficient to complete necessary evacuations, fatalities and injuries should be minimal. That leaves the metrics of affected population and(or) cost of the damage as perhaps a useful starting point.

5 Conclusions—the next steps

Ideally, a single system or model (likely a system of systems) could use the impactor parameters (such as mass, structure, impact location, and time and date) to determine the range and timing of all effects, including cascading effects. Most of the cascading effects are dependent on weather patterns that vary significantly—resulting in not a unique answer, but a probability distribution. Due to uncertainties in observed and derived asteroid properties, probability distributions are already being used for the initial effects of an impact or airburst. But even a probability distribution of cascading hazards would provide emergency and resource managers a new tool for planning, evacuation, and recovery efforts.

A single grand unified model is likely years, if not decades, away. Many of the cascading hazards depend on nonlinear complex processes which depend on variable environmental conditions to trigger the effect (e.g., high winds for resuspension or extreme precipitation for debris flows). Regardless, substantial progress can be made by coupling existing models of hazards in a cascading chain of effects. A probabilistic approach (e.g., Monte Carlo) is currently being used to estimate effects from the initial impact (e.g. PAIR, Mathias et al. 2017) and a similar approach could be used for cascading effects. These coupled models could be validated against more common natural hazards that also lead to a cascade of hazards, including volcanic eruptions and large earthquakes. With the increase in the number and intensity of wildfires, these also provide a means for cascading model validation.

We have identified and reviewed several of the current models for downstream (or down-flow) and downwind (or down-blow) events. These models can be interfaced by deriving the input parameters for these models from the output from the impact and airburst models. For example, the determination of resulting debris, dust and ash production, composition, and grain-size profiles are important inputs in both down-flow and down-blow models. However, current models of the initial effects of an asteroid impact do not

provide sufficiently granular properties and distributions of these parameters as part of their standard output. Additional modeling is needed to convert bulk destruction and debris estimates into distribution of debris and dust—including size. Until then, assumptions will need to be made to link these models.

As the global climate continues to change, with more widespread and longer-lasting drought, hotter temperatures, and more extreme weather, chained models of cascading hazards may be required for even minimally adequate response and recovery efforts to occur. Emergency response and recovery plans needing to be integrated as the result of cascading hazards, displaced in either space or time, will mean that mitigation and recovery responses no longer have the luxury of being linear.

Being prepared is key to minimizing the impact on life, property, and the economy for any large-scale disaster. We must first recognize when cascading hazards become important. The impactor size and mass at which there is a transition from local to region effects is not well constrained. We need to know when these delayed effects need to be considered in civil defense planning and when they can be ignored. Our actions, if not appropriate and informed, can be needlessly counter-productive for long-term mitigation and significantly increase the cost and loss of both life and property.

Acknowledgements We would like to thank Lorien Wheeler, Kaj Williams, and three anonymous reviewers for their insightful reviews and suggestions which greatly improved this article.

Funding This work was partially funded by NASA's Planetary Defense Coordination Office (PDCO). Resources supporting this work were provided by the NASA High-End Computing (HEC) Program through the NASA Advanced Supercomputing (NAS) Division at Ames Research Center.

Declarations

Conflict of interest The authors have no conflicts of interest to declare that are relevant to the content of this paper.

References

- Abdolzadeh M, Nikkiah R (2019) Experimental study of dust deposition settled over tilted PV modules fixed in different directions in the southeast of Iran. *Environ Sci Pollut Res* 26(30):31478–31490
- Aftosmis M, Nemec M, Mathias D, Berger M (2016) Numerical simulation of bolide entry with ground footprint prediction AIAA 2016–0998. *SciTech*. <https://doi.org/10.2514/6.2016-0998>
- Aftosmis MJ, Mathias DL, Tarano AM (2019) Simulation-based height of burst map for asteroid airburst damage prediction. *Acta Astronaut* 156:278–283
- Al Hemoud A, Al Dousari A, Misak R, Al-Sudairawi M, Naseeb A, Al-Dashti H, Al-Dousari N (2019) Economic impact and risk assessment of sand and dust storms (SDS) on the oil and gas industry in Kuwait. *Sustainability* 11(200):1–19
- Alsweiss S, Hanna R, Laupattarakasem P, Jones W, Hennon C, Chen R (2014) A non-MLE approach for satellite scatterometer wind vector retrievals in tropical cyclones. *Remote Sens* 6:4133–4148
- Alvarez LW, Alvarez W, Asaro F, Michel HV (1980) Extraterrestrial cause for the cretaceous-tertiary extinction. *Science* 208(4448):1095
- Anenberg SC, Horowitz LW, Tong DQ, West JJ (2010) An estimate of the global burden of anthropogenic ozone and fine particulate matter on premature human mortality using atmospheric modeling. *Environ. Health Perspect* 118(9):1189–1195. <https://doi.org/10.1289/ehp.0901220>
- Angell JK, Korshover J (1985) Surface temperature changes following the six major volcanic episodes between 1780 and 1980. *J Appl Meteorol Climatol* 24(9):937–951
- Arocena J, Opio C (2003) Prescribed fire-induced changes in properties of sub-boreal forest soils. *Geoderma* 113(1):1e16
- Artemieva N, Shuvalov V (2016) From Tunguska to Chelyabinsk via Jupiter. *Ann Rev Earth Planetary Sci* 44:37–56

- Artemieva N, Shuvalov V, Khazins V (2019) Upper atmosphere effects after the entry of small cosmic bodies: dust trains, plumes, and atmospheric disturbances. *Icarus* 327:60–71
- Atkinson G, Wald D (2007) “Did you feel it?” intensity data: a surprisingly good measure of earthquake ground motion. *Seismol Res Lett* 78(3):362–368
- Baars H, Radenz M, Floutsi AA et al (2021) Californian wildfire smoke over Europe: a first example of the aerosol observing capabilities of Aeolus compared to ground based lidar. *Geophys Res Lett* 48(8):e2020GL092194. <https://doi.org/10.1029/2020GL092194>
- Bardeen CG, Garcia RR, Toon OB, Conley AJ (2017) On transient climate change at the Cretaceous–paleogene boundary due to atmospheric soot injections. *Proc Natl Acad Sci* 114(36):7415
- Barnhart KR, Jones RP, George DL, McArdell BW, Rengers FK, Staley DM, Kean JW (2021) Multi-model comparison of computed debris flow runout for the 9 January 2018 Montecito, CA post-wildfire event. *J Geophys Res Earth Surf* 126(12):e06245
- Barnum BH, Winstead NS, Wesely J, Hakola A, Colarco PR, Toon OB, Ginoux P, Brooks G, Hasselbarth L, Toth B (2004) Forecasting dust storms using the CARMA-dust model and MM5 weather data. *Environ Model Softw* 19:129–140
- Behrouzi M, Bazgeer S, Nouri H, Nejatian MA, Akhzari D (2019) Dust storms detection and its impacts on the growth and reproductive traits of grape vine (*Vitis vinifera*) in Malayer plain. *Desert Ecosyst Eng J* 8(23):59–72
- Benjamin SG, Weygandt SS, Brown JM, Hu M, Alexander CR, Smirnova TG, Olsen JB, James EP, Dwell DC, Grel GA, Lin H, Peckham SE, Smith TL, Moninger WR, Kenyon JS (2016) A North American hourly assimilation and model forecast cycle: the rapid refresh. *Mon Wea Rev* 144:1669–1694
- Benmenni M, Benrachedi K (2010) Impact of earthquake demolition debris on the quality of groundwater. *Am J Appl Sci* 7(4):545–550
- Berger MJ, George DL, LeVeque RJ, Mandli KM (2011) The GeoClaw software for depth-averaged flows with adaptive refinement. *Adv Water Resour* 34:1195–1206
- Berger M, LeVeque R (2018) Modeling issues in asteroid-generated tsunamis. NASA. <https://ntrs.nasa.gov/api/citations/20180006617/downloads/20180006617.pdf>
- Bernstein RS, Baxter PJ, Falk H, Ing R, Foster L, Frost F (1986). Immediate public health concerns and actions in volcanic eruptions: lessons from the Mount St. Helens eruptions. *Am J Public Health* 76(Suppl):25–37. <https://doi.org/10.2105/AJPH.76.Suppl.25>
- Birjandi-Feriz M, Yousefi K (2017) When the dust settles: productivity and economic losses following dust storms. SSRN. <https://doi.org/10.2139/ssrn.3230265>
- Blake MD, Wilson MT, Cole WJ, Deligne IN, Lindsay MJ (2017) Impact of volcanic ash on road and airfield surface skid resistance. *Sustainability* 9(8):1389. <https://doi.org/10.3390/su9081389>
- Blong RJ (1984) *Volcanic Hazards*. Academic Press, Sydney, p 424
- Bonadonna C, Mayberry GC, Calder ES, Sparks RSJ, Choux C, Jackson AM, Lejeune AM, Loughlin SC, Norton GE, Rose WI, Ryan G, Young SR (2002) Tephra fallout in the eruption of Soufrière Hills Volcano, Montserrat. In: Druitt TH, Kokelaar BP (eds) *The eruption of Soufrière Hills Volcano, Montserrat, from 1995 to 1999*. Geological Society of London, London, pp 483–516
- Bormann P, Wendt S, DiGiacomo D (2013) Seismic sources and source parameters. Chapter in, *New manual of seismological observatory practice* 2. Ed. Bormann. Deutsches GeoForschungsZentrum, 1–259.
- Boslough M, Crawford D (1997) Shoemaker-Levy 9 and plume forming collisions on Earth. Proc. International conference on near-Earth objects, New York, New York, USA. Edited by John L. Remo. *Annals of the New York Academy of Sciences* v. 822, p.236.
- Boslough M, Crawford D (2008) Low-altitude airbursts and the impact threat. *Int J Impact Eng* 35:1441–1448
- Bradley RS (1988) The explosive volcanic eruption signal in northern hemisphere continental temperature records. *Clim Change* 12(3):221–243. <https://doi.org/10.1007/BF00139431>
- Bralower T, Paull C, Leckie R (1998) The Cretaceous-tertiary boundary cocktail: Chicxulub impact triggers margin collapse and extensive sediment gravity flows. *Geology* 26(4):331–334
- Brett R (1992) The Cretaceous-tertiary extinction: a lethal mechanism involving anhydrite target rocks. *Geochim Cosmochim Acta* 56(9):3603–3606
- Bursik MI, Carbonara AU, Zawicki SM, Patra A, Jones-Ivey R (2013) Puffin. <https://vhub.org/resources/puffin>
- Busse MD, Shestak CJ, Hubbert KR, Knapp EE (2010) Soil physical properties regulate lethal heating during burning of woody residues. *Soil Sci Soc Am J* 74(3):947955
- Campbell G, Jungbauer J Jr, Bristow KL, Hungerford R (1995) Soil temperature and water content beneath a surface fire. *Soil Sci* 159(6):363e374

- Carey S, Sigurdsson H (1986) The 1982 eruptions of El Chichon volcano, Mexico (2): observations and numerical modelling of tephra-fall distribution. *Bull Volcanol* 48(2–3):127–141
- Carey S, Sigurdsson H (1989) The intensity of plinian eruptions. *Bull Volcanol* 51(1):28–40
- Carn SA, Clarisse L, Prata AJ (2016) Multi-decadal satellite measurements of global volcanic degassing. *J Volcanol Geoth Res* 311:99–134
- Celano F, Dolšek M (2021) Fatality risk estimation for industrialized urban areas considering multi-hazard domino effects triggered by earthquakes. *Reliab Eng Syst Saf* 206:107287
- National Centers for Atmospheric Prediction. Global Forecast System (GFS): National Oceanic and Atmosphere Administration. Accessed October 1, 2021 at <https://www.ncdc.noaa.gov/data-access/model-data/model-datasets/global-forecast-system-gfs>.
- Cerdà A, Doerr SH (2005) Influence of vegetation recovery on soil hydrology and erodibility following fire: an 11-year investigation. *Int J Wildland Fire* 14(4):423–437. <https://doi.org/10.1071/WF05044>
- Certini G (2005) Effects of fire on properties of forest soils: a review. *Oecologia* 143(1):1–10
- Chandler C, Williams D, Trabaud L, Thomas P, Cheney P (1983) *Fire in Forestry: Forest Fire Behavior and Effects*. John Wiley and Sons, New York
- Chapin FS III, Matson PA, Mooney HA (2002) *Principles of terrestrial ecosystem ecology*. Springer-Verlag
- Chesley S, Ward S (2006) A quantitative assessment of the human and economic hazard from impact-generated tsunamis. *Nat Hazards* 38:355–374
- Chief K, Young MH, Shafer DS (2012) Changes in soil structure and hydraulic properties in a wooded-shrubland ecosystem following a prescribed fire. *Soil Sci Soc Am J* 76(6):1965–1977
- Chyba C, Thomas P, Zahnle K (1993) The 1908 Tunguska explosion; atmospheric disruption of a stony asteroid. *Nature* 301:40–44
- Coates, A, Stern, E, Johnston, C, Wheeler, L, Mathias, D (2021) Comparison of thermal radiation damage models and parameters for impact risk assessment. *7th IAA Planetary Defense Conference*.
- Collins G, Melosh H, Marcus R (2005) Earth impact effects program: a web-based computer program for calculating the regional environmental consequences of a meteoroid impact on Earth. *Meteorit Planet Sci* 40(6):817–840
- Collins GS, Patel N, Davison TM, et al. (2020) A steeply-inclined trajectory for the Chicxulub impact. *Nat Commun* 11:1480. <https://doi.org/10.1038/s41467-020-15269-x>
- Cook RJ, Barron JC, Papendick RI, Williams GJ (1981) Impact on agriculture of the Mount St. Helens eruptions. *Science* 211(4477):16–22
- Coupe J, Bardeen C, Robock A, Toon OB (2019) Nuclear winter responses to nuclear war between the United States and Russia in the whole atmosphere community climate model version 4 and the goddard institute for space studies model. *J Geophys Res* 124:8522–8543
- Covey C, Thompson SL, Weissman PR, MacCracken MC (1994) Global climatic effects of atmospheric dust from an asteroid or comet impact on earth. *Global Planet Change* 9(3):263–273
- Czajkowski J, Kennedy E (2010) Fatal tradeoff? toward a better understanding of the costs of not evacuating from a hurricane in landfall counties. *Popul Environ* 31:121–149
- DeBano LF (2000) The role of fire and soil heating on water repellency in wildland environments: a review. *J Hydrol* 231:195–206. [https://doi.org/10.1016/S0022-1694\(00\)00194-3](https://doi.org/10.1016/S0022-1694(00)00194-3)
- DeBano LF, Rice RM, Eugene CC (1979) *Soil heating in chaparral fires: Effects on soil properties, plant nutrients, erosion, and runoff*. Tech. Rep. Berkeley, CA: U.S. Forest Service Research Paper (RP-145).
- DePalma R, Smit J, Burnham D, Kuiper K, Manning P, Oleinik A, Larson P, Maurrasse F, Vellekoop J, Richards M, Gurche L, Alvarez W (2019) A seismically induced onshore surge deposit at the KPg boundary, North Dakota. *Proc Natl Acad Sci USA* 116(17):8190–8199
- Dong Z, Chen G, He X, Han Z, Wang X (2002) Controlling blown sand along the highway crossing the taklimakan desert. *J Arid Environ* 57(2004):329–344
- Van Dorn W, Le Mehaute B, Hwang L (1968) *Handbook of explosion-generated water waves*. Office of Naval Research, Virginia
- Dragoni M, Santoro D (2020) A model for the atmospheric shock wave produced by a strong volcanic explosion. *Geophys J Int* 222(2):735–742. <https://doi.org/10.1093/gji/ggaa205>
- Dukes D, Gonzales HB, Ravi S, Grandstaff DE, Scott Van Pelt R, Li J, Wang G, Sankey JB (2018) Quantifying postfire aeolian sediment transport using rare earth element tracers, JGR. *Biogeosciences* 123(1):288–299
- Duncombe J (2021) Climate change and extreme weather linked in U.N. climate report. *Eos*. <https://doi.org/10.1029/2021EO162326>
- Dutton EG, Christy JR (1992) Solar radiative forcing at selected locations and evidence for global lower tropospheric cooling following the eruptions of El Chichón and Pinatubo. *Geophys Res Lett* 19(23):2313–2316. <https://doi.org/10.1029/92GL02495>

- Ebel BA (2020) Temporal evolution of measured and simulated infiltration following wildfire in the Colorado front range, USA: shifting thresholds of runoff generation and hydrologic hazards. *J Hydrol* 585:124765. <https://doi.org/10.1016/j.jhydrol.2020.124765>
- Ebel BA, Rengers FK, Tucker GE (2016) Observed and simulated hydrologic response for a first-order catchment during extreme rainfall 3 years after wildfire disturbance. *Water Resour Res*. <https://doi.org/10.1002/2016WR019110>
- Elliot WJ, Miller IS, Glaza BD (2006) Using WEPP Technology to Predict Erosion and Runoff Following Wildfire. An ASABE Meeting Presentation Paper Number: 06801. <https://forest.moscowfsl.wsu.edu/engr/library/Elliot/Elliot2006g/2006g.pdf>
- EPA (2019) Planning for natural disaster debris, EPA 530-F-19-003. https://www.epa.gov/sites/default/files/2019-04/documents/final_pndd_guidance_0.pdf
- Fairfield C (1980) OMSI sound project: the acoustic effects of the Mount St. Helens eruption on May 18, 1980. *Or Geol* 42(12):200–203
- Fan X, van Westen C, Korup O, Gorum T, Xu Q, Dai F, Huang R, Wang G (2012) Transient water and sediment storage of the decaying landslide dams induced by the 2008 Wenchuan earthquake, China. *Geomorphology* 171–172:58–68
- Fan X, Scaringi G, Korup O, West AJ, van Westen CJ, Tanyas H, Hovius N, Hales T, Jibson R, Allstadt K, Zhang L, Evans S, Xu C, Li G, Pei X, Xu Q, Huang R (2018) Earthquake-induced chains of geologic hazards: patterns, mechanisms, and impacts. *Rev Geophys* 57(2):421–503
- Fan X, Yunus AP, Scaringi G, Catani F, Subramanian SS, Xu Q, Huang R (2021) Rapidly evolving controls of landslides after a strong earthquake and implications for hazard assessments. *Geophys Res Lett* 48(1):E90509
- Fann N, Alman B, Broome RA, Morgan GG, Johnston FH, Pouliot, G., & Rappold, A.G. (2017). The health impacts and economic value of wildland fire episodes in the U.S.: 2008–2012. *Science of the Total Environment* 610–611:802–809. <https://doi.org/10.1016/j.scitotenv.2017.08.024>
- Farmer A (1993) The effects of dust on vegetation—a review. *Environ Pollut* 79:63–75
- Fast V (1967) Statistical analysis of parameters of the Tunguska tree-fall. *Problems of the Tunguska Meteorite*. Tomsk University Press, Tomsk, pp 40–61
- Fitzpatrick R (1980) Effect of forest and grass burning on mineralogical transformations in some soils of natal. *Soil Irrigat Res Inst Rep* 952(139):80
- Folch A, Mingari L, Gutierrez N, Hanzich M, Macedonio G, Costa A (2020) FALL3D-8.0: a computational model for atmospheric transport and deposition of particles, aerosols and radionuclides—part 1: model physics and numerics. *Geosci Model Dev* 13(3):1431–1458
- George DL, Iverson RM (2014) A depth-averaged debris-flow model that includes the effects of evolving dilatancy. II. Numerical predictions and experimental tests. *Proceedings of the Royal Society A: Mathematical, Physical and Engineering Science* 470(2170). <http://rspa.royalsocietypublishing.org/content/royprsa/470/2170/20130820.full.pdf>
- Gladysheva OG (2012) Atmospheric anomalies in the summer of 1908: skyglow. *Geomag Aeron* 52(4):526–532. <https://doi.org/10.1134/s001679321203005x>
- Glasstone S, Dolan P (1977) *The Effects of Nuclear Weapons*. Department of Defense and the Energy Research and Development Administration, United States
- Glazachev DO, Popova OP, Podobnaya ED, Artemieva NA, Shuvalov VV, Svetsov VV (2021) Shock wave effects from the impacts of cosmic objects with diameters from 20 m to 3 km *Izvestiya. Phys Solid Earth* 57(5):698–709
- Goodrich DC, Burns IS, Unkrich CL, Semmens DJ, Guertin DP, Hernandez M (2012) KINEROS2/AGWA: model use, calibration, and validation. *Trans ASABE* 55(4):1561–1574. <https://doi.org/10.13031/2013.42264>
- Gorkavyy N, Rault D, Newman P, da Silva A, Dudorov A (2013) New stratospheric dust belt due to the Chelyabinsk bolide. *Geophys Res Lett* 40:4728–4733
- Gran KB, Montgomery DR, Halbur JC (2011) Long-term elevated post-eruption sedimentation at mount pinatubo, philippines. *Geol* 39(4):367–370. <https://doi.org/10.1130/g31682.1>
- Han I, Whitworth KW, Christensen B et al (2022) Heavy metal pollution of soils and risk assessment in houston, texas following hurricane harvey. *Environ Pollut* 296:118717. <https://doi.org/10.1016/j.envpol.2021.118717>
- Harkrider D, Press F (1967) The krakatoa air—sea waves: an example of pulse propagation in coupled systems. *Geophys J Int* 13(1–3):149–159. <https://doi.org/10.1111/j.1365-246X.1967.tb02150.x>
- Hasselquist NJ, Germino MJ, Sankey JB, Ingram LJ, Glenn NF (2011) Aeolian nutrient fluxes following wildfire in sagebrush steppe: implications for soil carbon storage. *Biogeosciences* 8:3649–3659. <https://doi.org/10.5194/bg-8-3649-2011>

- Hawkins RH, Munoz AB (2011) Wildcat5 for Windows (W5W): Documentation and Manual. University of Arizona, Tucson, Arizona, School of Natural Resources and Environment
- Hills J, Goda M (1993) The fragmentation of small asteroids in the atmosphere. *Astron J* 105(3):1114–1144
- Hills J, Goda M (1999) Damage from comet-asteroid impacts with earth. *Phys D* 133:189–198
- Hungerford RD, Harrington MG, Frandsen WH, Ryan KC, Niehoff GJ (1991) Influence of fire on factors that affect site productivity. In: Proceedings of the symposium on management and productivity of Western-Montane forest soils, pp. 32–50.
- Iverson RM, Schilling SP, Vallance JW (1998) Objective delineation of lahar-inundation hazard zones. *GSA Bull* 110(8):972–984. [https://doi.org/10.1130/0016-7606\(1998\)110%3c0972:ODOLIH%3e2.3.CO;2](https://doi.org/10.1130/0016-7606(1998)110%3c0972:ODOLIH%3e2.3.CO;2)
- Iverson RM, George DL (2014) A depth-averaged debris-flow model that includes the effects of evolving dilatancy. I. Physical basis. *Proceedings of the Royal Society A: Mathematical, Physical and Engineering Science* 470(2170). <http://rspa.royalsocietypublishing.org/content/royprsa/470/2170/20130819.full.pdf>
- Jackson M, Roering J (2009) Post-fire geomorphic response in steep, forested landscapes: oregon coast range, USA. *Quatern Sci Rev* 28:1131–1146. <https://doi.org/10.1016/j.quascirev.2008.05.003>
- Jaiswal K, Wald D, Hearne M (2009) Estimating casualties for large earthquakes worldwide using an empirical approach. *U.S. Geological Survey*, 2009–1136.
- Jenni KE, Goldhaber MB, Betancourt JL et al (2017) Grand challenges for integrated U.S. Geological Survey science—A workshop report: U.S. Geological Survey Open-File Report 2017–1076, 94 p. <https://doi.org/10.3133/ofr20171076>
- Jenniskens P, Popova O, Glazachev D, Podobnaya E, Kartashova A (2019) Tunguska eyewitness accounts, injuries, and casualties. *Icarus* 327:4–18. <https://doi.org/10.1016/j.icarus.2019.01.001>
- Jibson RW, Allstadt KE, Rengers FK, Godt JW (2017) Overview of the geologic effects of the November 14, 2016 Mw 7.8 Kaikoura, New Zealand, earthquake: US. Geological Survey Scientific Investigations Report <https://doi.org/10.3133/sir20175146>.
- Johnston C, Stern E (2019) A model for the thermal radiation from the Tunguska airburst. *Icarus* 327:48–59
- Johnston C, Stern E, Wheeler L (2018) Radiative heating of large meteoroids during atmospheric entry. *Icarus* 309:25–44
- Jones A, Thomson D, Hort M, Devenish B (2007) The U.K. Met Office's Next-Generation Atmospheric Dispersion Model, NAME III. In: Borrego C, Norman A-L (eds) *Air Pollution Modeling and Its Application XVII*. Springer, Berlin, pp 580–589
- Jonkman S, Vrijling J, Vrouwenvelder A (2008) Methods for the estimation of loss of life due to floods: a literature review and a proposal for a new method. *Nat Hazards* 46:353–389
- Jutzi M, Holsapple K, Winneman K, Michel P (2015) Modeling asteroid collisions and impact processes. In: Meo FE, Bottke WF, Michel P (eds) *Asteroids*. University of Arizona Press, Arizona
- Kalnay E, Kanamitsu M, Kistler R, Collins W, Deaven D, Gandin L, Iredell M, Saha S, White G, Woolen J, Zhu Y, Leetmaa A, Reynolds R, Chelliah M, Ebisuzak W, Higgins W, Janowiak J, Mo KC, Ropelewski C, Wang J, Jenne R, Joseph D (1996) The NCEP/NCAR 40-year reanalysis project. *Bull Am Meteor Soc* 77(3):437–471. <https://doi.org/10.1175/1520-0477>
- Kasatkina E, Shumilov O (2007) One more puzzle of the Tunguska catastrophe? *J Exp Theor Phys Lett* 85(4):216–219. <https://doi.org/10.1134/S0021364007040078>
- Kaufmann W (1908) Leuchtende Wolke (Luminous cloud). (In German) *Physikalische Zeitschrift* 9(18).
- Kean JW, McGuire LA, Rengers FK, Smith JB, Staley DM (2016) Amplification of postwildfire peak flow by debris. *Geophys Res Lett* 43:8545–8553. <https://doi.org/10.1002/2016GL069661>
- Kelley CP, Mohtadi S, Cane MA, Seager R, Kushnir Y (2015) Climate change in the fertile crescent and implications of the recent Syrian drought. *Proc Natl Acad Sci USA* 112(11):3241–3246. <https://doi.org/10.1073/pnas.1421533112>
- Khaykin S, Legras B, Bucci S, Sellitto P, Isaksen I, Tencé F, Bekki S, Bourassa A, Rieger L, Zawada D, Jumelet J, Godin-Beekmann S (2020) The 2019/20 Australian wildfires generated a persistent smoke-charged vortex rising up to 35 km altitude. *Commun Earth Environ* 1(1):22. <https://doi.org/10.1038/s43247-020-00022-5>
- Khazins V, Shuvalov V, Svetstov V (2018) The seismic efficiency of space body impacts. *Sol Syst Res* 52(6):547–556
- Kieffer SW (1981) Blast dynamics at Mount St. Helens on 18 May 1980. *Nature* 291:568–570
- Kinoshita AM, Hogue TS, Napper C (2014) Evaluating pre-and post-fire peak discharge predictions across western US watersheds. *J Am Water Resour Assoc* 50(6):1540–1557
- Korycanski D, Lynett P (2005) Offshore breaking of impact tsunamis: the Van Dorn effect revisited. *Geophys Res Lett* 32:L10608
- Korycanski D, Lynett P (2007) Run-up from impact tsunamis. *Geophys J Int* 170(3):1076–1088

- Koshimura S, Oie T, Yanagisawa H, Imamura F (2009) Developing fragility functions for tsunami damage estimation using numerical model and post-tsunami data from Banda Aceh Indonesia. *Coast Eng J* 51(3):243–273
- Koyaguchi T, Tokuno M (1993) Origin of the giant eruption cloud of Pinatubo, June 15, 1991. *J Volcanol Geoth Res* 55:85–96
- Krajickova A, Mejstrik V (1984) The effect of fly-ash particles on the plugging of stomata. *Environ Poll* 36:83–93
- Kring D, Durda D (2002) Trajectories and distribution of material ejected from the Chicxulub impact crater: Implications for postimpact wildfires. *J Geophys Res* 107(E8):5062. <https://doi.org/10.1029/2001J E001532>
- Kring D, Durda D (2004) Trajectories and distribution of material ejected from the Chicxulub impact crater: implications for postimpact wildfires. *J Geophys Res* 107(E8–5062):6–1
- Langhans C, Smith HG, Chong DM, Nyman P, Lane PN, Sheridan GJ (2016) A model for assessing water quality risk in catchments prone to wildfire. *J Hydrol* 534:407–426
- Larsen IJ, MacDonald LH, Brown E, Rough D, Welsh MJ, Pietraszek JH et al (2009) Causes of post-fire runoff and erosion: Water repellency, cover, or soil sealing? *Soil Sci Soc Am J* 73(4):1393–1407. <https://doi.org/10.2136/sssaj2007.0432>
- Lee JA, Gill TE (2015) Multiple causes of wind erosion in the dust bowl. *Aeolian Res* 19:15–36. <https://doi.org/10.1016/j.aeolia.2015.09.002>
- Lelieveld J, Evans JS, Fnais M, Giannadaki D, Pozzer A (2015) The contribution of outdoor air pollution sources to premature mortality on a global scale. *Nat* 525(7569):367–371. <https://doi.org/10.1038/nature15371>
- Lindell M, Prater C, Perry R, Nicholson W (2006) Fundamentals of Emergency Management. *US Federal Emergency Management Agency*.
- Liu T, McGuire LA, Oakley N, Cannon F (2022) Temporal changes in rainfall intensity-duration thresholds for post-wildfire flash floods in southern California. *Nat Hazards Earth Syst Sci* 22(2):361–376
- Løvholt F, Pedersen G, Gislser G (2008) Oceanic propagation of a potential tsunami from the La Palma Island. *J Geophys Res* 113:C09026
- Løvholt F, Pedersen G, Harbitz C, Glimsdal S, Kim J (2015) On the characteristics of landslide tsunamis. *Phil Trans R Soc A* 373:20140376
- Macedonio G, Costa A, Longo A (2005) A computer model for volcanic ash fallout and assessment of subsequent hazard. *Comput Geosci* 31(7):837–845. <https://doi.org/10.1016/j.cageo.2005.01.013>
- Mannan S (2005) Lee's loss prevention in the process industries, 3rd edn. Elsevier
- Marson SM, Legerton M (2021) Disaster diaspora and the consequences of economic displacement and climate disruption, including hurricanes matthew (october 8, 2016) and florence (september 14, 2018) in robeson county North Carolina. *Nat Hazards* 107:2247–2262. <https://doi.org/10.1007/s11069-021-04529-8>
- Mason BG, Pyle DM, Oppenheimer C (2004) The size and frequency of the largest explosive eruptions on Earth. *Bull Volcanol* 66:735–748. <https://doi.org/10.1007/s00445-004-0355-9>
- Massey C, Townsend D, Rathje E, Kaneko Y, Lukovic B, Horspool N, Bradley B, Hamling I, Wartman J, Allstadt K, Carey J, Cox S, Davidson J, Dellow S, Holden C, Jones K, Kaiser A, Lyndsell B, McColl S, Morgenstern R, Petley DN, Rhoades D, Rosser B, Strong D, Singeisen C, Villeneuve M, Rengers FK (2018) Landslides triggered by the 14 november 2016, MW 7.8 kaikoura earthquake, New Zealand. *Bull Seismol Soc Am* 108(3B):1630–1648. <https://doi.org/10.1785/0120170305>
- Massman W, Frank J, Shepperd W, Platten M, Omi PN, Joyce LA (2003) In situ soil temperature and heat flux measurements during controlled surface burns at a southern Colorado forest site. In: *USDA Forest Service Proceedings, RMRS-P-29 (Fort Collins, CO)*.
- Mastin LG, Guffanti M, Servranckx R, Webley P, Barsotti S, Dean K, Durant A, Ewert JW, Neri A, Rose WI, Schneider D, Siebert L, Stunder B, Swanson G, Tupper A, Volentik A, Waythomas CF (2009) A multidisciplinary effort to assign realistic source parameters to models of volcanic ash-cloud transport and dispersion during eruptions. *J Volcanol Geoth Res* 186(1–2):10–21
- Mastin LG, Randall MJ, Schwaiger HF, Denlinger RP (2013) User's guide and reference to Ash3d: A Three-Dimensional Model for Atmospheric Tephra Transport and Deposition. *U.S. Geological Survey. Open-File Report* 2013–1122, 48 p., <http://pubs.usgs.gov/of/2013/1122/>.
- Mathias D, Wheeler L, Dotson J (2017) A probabilistic asteroid impact risk model: assessment of sub-300 m impacts. *Icarus* 289:106–119. <https://doi.org/10.1016/j.icarus.2017.02.009>
- McCrea PR (1984) An assessment of the effects of road dust on agricultural production systems, Research Report No. 156 ISSN 0069–3790. https://rcaforum.org.nz/sites/public_files/images/Effects%20of%20road%20dust-McCrea-1984-rr156.pdf

- McGuire LA, Kean JW, Staley DM, Rengers FK, Wasklewicz TA (2016) Constraining the relative importance of raindrop- and flow-driven sediment transport mechanisms in postwildfire environments and implications for recovery time scales. *J Geophys Res Earth Surf* 121:2211–2237. <https://doi.org/10.1002/2016JF003867>
- McGuire LA, Rengers FK, Kean JW, Staley DM (2017) Debris flow initiation by runoff in a recently burned basin: Is grain-by-grain sediment bulking or en masse failure to blame? *Geophys Res Lett* 44(14):7310–7319. <https://doi.org/10.1002/2017GL074243>
- McGuire LA, Rengers FK, Kean JW, Staley DM, Mirus BB (2018) Incorporating spatially heterogeneous infiltration capacity into hydrologic models with applications for simulating post-wildfire debris flow initiation. *Hydrol Process* 32(9):1173–1187
- McMullan S, Collins G (2019) Uncertainty quantification in continuous fragmentation airburst models. *Icarus* 327:19–35
- McMullan S (2020) Numerical modelling of meteoroid airbursts. *Ph.D. thesis*, Imperial College, London.
- Le Mehaute B, Wang S (1996) Water waves generated by underwater explosions. Defense Nuclear Agency.
- Meibodi AE, Abdoli G, Taklif A, Morshedi B (2015) Economic modeling of the regional policies to combat dust phenomenon by using game theory. *Proc Econ Fin* 24:409–418. [https://doi.org/10.1016/S2212-5671\(15\)00697-8](https://doi.org/10.1016/S2212-5671(15)00697-8)
- Melosh JJ, Vickery AM (1991) Melt droplet formation in energetic impact events. *Nature* 350(6318):494–497. <https://doi.org/10.1038/350494a0>
- Melosh H, Schneider N, Zahnle K, Latham D (1990) Ignition of global wildfires at the cretaceous/tertiary boundary. *Nature* 343:251
- Mercado RA, Bertram J, Lacsamana T, Pineda GL (1995) Socioeconomic Impacts of the Mount Pinatubo Eruption. In: Newhall C, Punongbayan R (eds) *Fire and Mud: Eruptions and Lahars of Mount Pinatubo*, Philippines. University of Washington Press, Seattle, WA, pp 1063–1070
- Miller ME, Bowker MA, Reynolds RL, Goldstein HL (2012) Post-fire land treatments and wind erosion—lessons from the Milford Flat Fire, UT, USA. *Aeolian Res* 7:29–44
- Miller ME, MacDonald LH, Robichaud PR, Elliot WJ (2011) Predicting post-fire hillslope erosion in forest lands of the western United States. *Int J Wildland Fire* 20:982–999
- Moody J, Ebel B (2012) Hyper-dry conditions provide new insights into the cause of extreme floods after wildfire. *CATENA* 93:58–63. <https://doi.org/10.1016/j.catena.2012.01.006>
- Moody JA, Ebel BA (2014) Infiltration and runoff generation processes in fire-affected soils. *Hydrol Process* 28(9):3432–3453. <https://doi.org/10.1002/hyp.9857>
- Moody JA, Martin DA (2009) Synthesis of sediment yields after wildland fire in different rainfall regimes in the western United States. *Int J Wildland Fire* 18:96–115
- Moody JA, Dungan Smith J, Ragan BW (2005) Critical shear stress for erosion of cohesive soils subjected to temperatures typical of wild- fires. *J Geophys Res Earth Surf* 110(F01004):1–13. <https://doi.org/10.1029/2004JF000141>
- Moradi A, Taheri Abkenar K, Afshar Mohammadian M, Shabaniyan N (2017) Effects of dust on forest tree health in Zagros oak forests. *Environ Monit Assess* 189(11):549
- Morrison D, Harris AW, Sommer G, Chapman CR, Carusi A (2002) Dealing with the Impact Hazard, in *Asteroids III*, <https://www.lpi.usra.edu/books/AsteroidsIII/pdf/3043.pdf>
- Morrissey MM, Mastin LG (2000) Vulcanian eruptions. In: Sigurdsson H, Houghton BF, McNutt SR, Rymer H, Stix J (eds) *Encyclopedia of Volcanoes*. Academic Press, San Diego
- Moussa N, Devarakonda V (2014) Prediction of toxic emissions from chemical fire and explosion. *Fire Safety Science Proceedings 11th International Symposium*, pp. 1457–1468.
- Murphy SF, Writer JH, McCleskey RB, Martin DA (2015) The role of precipitation type, intensity, and spatial distribution in source water quality after wildfire. *Environ Res Lett* 10:1–13
- Myhre G, Shindell D, Bréon F-M, Collins W, Fuglestedt J, Huang J, Koch D, Lamarque J-F, Lee D, Mendoza B, Nakajima T, Robock A, Stephens G, Takemura T, Zhang H (2013) Anthropogenic and Natural Radiative Forcing. In: Stocker TF, Qin D, Plattner G-K, Tignor M, Allen SK, Boschung J, Nauels A, Xia Y, Bex V, Midgley PM (eds) *Climate Change 2013: The Physical Science Basis Contribution of Working Group I to the Fifth Assessment Report of the Intergovernmental Panel on Climate Change*. Cambridge University Press, Cambridge, U.K and New York U.S.A, p 1585
- Nairn I (1976) Atmospheric shock waves and condensation clouds from ngauruhoe explosive eruptions. *Nature* 259:190–192
- Nammah H, Larsen FE, McCool DK, Fritts R, Molnau M (1986) Mt. St. Helens volcanic ash: effect of incorporated and unincorporated ash of two particle sizes on runoff and erosion. *Agri Ecosyst Environ* 15(1):63–72

- National Environmental Satellite Data and Information Service (NESDIS), (2021), Earth from Orbit: Wildfire Smoke Blankets U.S. <https://www.nesdis.noaa.gov/news/earth-orbit-wildfire-smoke-blankets-us?msclid=f71c1594bb8a11ec877ddbc4e1e4f2a9>
- National Science and Technology Council (NSTC). (2018). National near-earth object preparedness strategy and action plan: a report by the interagency working group for detecting and mitigating the impact of earth-bound near-earth objects of the National science and technology council. <https://www.whitehouse.gov/wpcontent/uploads/2018/06/National-Near-Earth-Object-Preparedness-Strategy-and-Action-Plan-23-pages-1MB.pdf>.
- Newhall C, Punongbayan A (eds) (1996) Fire and mud: Eruptions and lahars of Mount Pinatubo. University of Washington Press, Philippines
- Newhall CG, Self S (1982) The volcanic explosivity index/VEI— an estimate of explosive magnitude for historical volcanism. *J Geophys Res* 87(C2):1231–1238. <https://doi.org/10.1029/JC087iC02p01231>
- Newhall C, Hendley J, Stauffer P (2005) The cataclysmic 1991 eruption of Mount Pinatubo. U.S. Geological Survey fact sheet, Philippines. <https://doi.org/10.1029/JC087iC02p01231>
- Nickovic S, Kallos G, Papadopoulos A, Kakaliagou O (2001) A model for prediction of desert dust cycle in the atmosphere. *J Geophys Res* 106(D16):18113–18130
- Niemeier U, Timmreck C, Graf HF, Kinne S, Rast S, Self S (2009) Initial fate of fine ash and sulfur from large volcanic eruptions. *Atmos Chem Phys* 9(22):9043–9057
- NOAA, National Hurricane Center, (2021) National hurricane center and central pacific hurricane center website, <https://www.nhc.noaa.gov/>.
- Noske PJ, Nyman P, Lane PN, Sheridan GJ (2016) Effects of aridity in controlling the magnitude of runoff and erosion after wildfire. *Water Resour Res* 52(6):4338–4357. <https://doi.org/10.1002/2015WR017611>
- Notaro M, Yu Y, Kalashnikova OV (2015) Regime shift in Arabian dust activity, triggered by persistent fertile crescent drought. *J Geophys Res Atmospheres* 120:10229–10249. <https://doi.org/10.1002/2015JD023855>
- Nyman P, Sheridan GJ, Lane PN (2013a) Hydro-geomorphic response models for burned areas and their applications in land management. *Prog Phys Geogr* 37(6):787–812
- Nyman P, Sheridan GJ, Moody JA, Smith HG, Noske PJ, Lane PN (2013b) Sediment availability on burned hillslopes. *J Geophys Res Earth Surf* 118(4):24512467
- Nyman P, Sheridan GJ, Smith HG, Lane PNJ (2014) Modeling the effects of surface storage, macropore flow and water repellency on infiltration after wildfire. *J Hydrol* 513:301–313. <https://doi.org/10.1016/j.jhydrol.2014.02.044>
- Ogburn SE, Norgaard D, Charlton D, Calder ES, Wright HM, Lindsay J, Takarada S, Ewert J (2020) Volcanic hazard maps database, v. 1.1 (20 September 2020). <https://volcanichazardmaps.org>. Accessed on 5 April 2022
- Okin GS, Gillette DA, Herrick JE (2006) Multi-scale controls on and consequences of aeolian processes in landscape change in arid and semi-arid environments. *J Arid Environ* 65:253–275
- Onda Y, Dietrich WE, Booker F (2008) Evolution of overland flow after a severe forest fire, point Reyes California. *CATENA* 72(1):13–20. <https://doi.org/10.1016/j.catena.2007.02.003>
- Oppenheimer C (2003) Climatic, environmental and human consequences of the largest known historic eruption: tambora volcano (Indonesia) 1815. *Progress Phys Geogr Earth Environ* 27(2):230–259. <https://doi.org/10.1191/0309133303pp379ra>
- Painter TH, Skiles SM, Deems JS, Brandt WT, Dozier J (2018) Variation in rising limb of colorado river snowmelt runoff hydrograph controlled by dust radiative forcing in snow. *Geophys Res Lett* 45(2):797–808. <https://doi.org/10.1002/2017GL075826>
- Palmieri A, Shah F, Dinar A (2001) Economics of reservoir sedimentation and sustainable management of dams. *J Environ Manag* 61:149–163. <https://doi.org/10.1006/jema.2000.0392>
- Pankhurst MJ, Stevenson CJ, Coldwell BC (2022) Meteorites that produce K-feldspar-rich ejecta blankets correspond to mass extinctions. *J Geol Soc*. <https://doi.org/10.1144/jgs2021-055>
- Parise M, Cannon S (2012) Wildfire impacts on the processes that generate debris flows in burned watersheds. *Nat Hazards* 61(1):217–227. <https://doi.org/10.1007/s11069-011-9769-9>
- Passey Q, Melosh H (1980) Effects of atmospheric breakup on crater field formation. *Icarus* 42(2):211–233
- PDC2021 (2021) The 2021 PDC Hypothetical Asteroid Impact Scenario, <https://cneos.jpl.nasa.gov/pd/cs/pdc21/>
- Pierce JL, Meyer GA, Jull AT (2004) Fire-induced erosion and millennial-scale climate change in northern ponderosa pine forests. *Nature* 432:87–90
- Pinatubo Volcano Observatory Team (1991) Lessons from a major eruption: Mt. Pinatubo Philippines. *EOS Trans Am Geophys Union* 72(49):545–555. <https://doi.org/10.1029/90EO00386>

- Pope CA, Ezzati M, Dockery DW (2009) Fine-particulate air pollution and life expectancy in the United States. *N Engl J Med* 360(4):376–386. <https://doi.org/10.1056/nejmsa0805646>
- Popova O, Jenniskens P, Emel'Yanenko V et al (2013) Chelyabinsk airburst, damage assessment, meteorite recovery, and characterization. *Science* 342(6162):1069–1073
- Popova O, Shuvalov V, Svetsov VKV, Artemieva N (2020) *Impact Effects*. [Online] Available at: <http://www.asteroidhazard.pro/>
- Prospero JM, Delany AC, Delany AC, Carlson TN (2021) The discovery of african dust transport to the western hemisphere and the saharan air layer: a history. *Bull Am Meteor Soc* 102(6):E1239–E1260
- Rahimi J, Ebrahimpour M, Khalili A (2013) Spatial changes of extended de martonne climatic zones affected by climate change in Iran. *Theoret Appl Climatol* 112:409–418
- Rappold AG, Fann NL, Crooks J, Huang J, Cascio WE, Devlin RB, Diaz-Sanchez D (2014) Forecast-based interventions can reduce the health and economic burden of wildfires. *Environ Sci Technol* 48(18):10,571–10,579. <https://doi.org/10.1021/es5012725>
- Rasch PJ, Mahowald NM, Eaton BE (1997) Representations of transport, convection, and the hydrologic cycle in chemical transport models: implications for the modeling of short-lived and soluble species. *J Geophys Res Atmos* 102(D23):28127–28138. <https://doi.org/10.1029/97JD02087>
- Rashki A, Middleton NJ, Goudie AS (2021) Dust storms in Iran—distribution, causes, frequencies and impacts. *Aeol Res* 48:100655. <https://doi.org/10.1016/j.aeolia.2020.100655>
- Ravi S, D'Odorico P, Breshears DD et al (2011) Aeolian processes and the biosphere. *Rev Geophys*. <https://doi.org/10.1029/2010RG000328>
- Ravia S, D'Odorico P, Zobeck TM, Over TM (2009) The effect of fire-induced soil hydrophobicity on wind erosion in a semiarid grassland: experimental observations and theoretical framework. *Geomorphol* 105(1–2):80–86
- Reed JW (1987) Air pressure waves from Mount St. Helens eruptions. *J Geophys Res Atmos* 92(D10):11979–11992. <https://doi.org/10.1029/JD092iD10p11979>
- Reid CE, Considine EM, Watson GL, Telesca D, Pfister GG, Jerrett M (2019) Associations between respiratory health and ozone and fine particulate matter during a wildfire event. *Environ Int* 129:291–298. <https://doi.org/10.1016/j.envint.2019.04.033>
- Reinhart D, McCreanor P (1999) Disaster debris management planning tools. *US Environmental Protection Agency* final report.
- Rengers FK, McGuire LA, Kean JW, Staley DM, Hogley DEJ (2016) Model simulations of flood and debris flow timing in steep catchments after wildfire. *Water Resour Res* 52(8):6041–6061. <https://doi.org/10.1002/2015WR018176>
- Rengers F, McGuire L, Kean J, Staley D, Youberg A (2019) Progress in simplifying hydrologic model parameterization for broad applications to post-wildfire flooding and debris-flow hazards. *Earth Surf Proc Land* 44(15):3078–3092. <https://doi.org/10.1002/esp.4697>
- Rengers FK, McGuire LA, Oakley NS, Tang H, Kean JW, Staley DM (2020) Landslides after Wildfire: initiation, magnitude, and mobility after fire. *Landslides* 17(11):2631–2641. <https://doi.org/10.1007/s10346-020-01506-3>
- Rengers FK, McGuire LA, Kean JW, Staley DM, Dobre M, Robichaud PR, Swetnam T (2021) Movement of sediment through a burned landscape: sediment volume observations and model comparisons in the San Gabriel Mountains, California, USA. *J Geophys Res Earth Surf* 126:e2020JF006053. <https://doi.org/10.1029/2020JF006053>
- Rengers FK, Pagonis V, Mahan SA (2017) Can thermoluminescence be used to determine soil heating from a wildfire?. *Radiat Meas* 107:119–127
- ReVelle D (2007) Fireball diversity: energetics-based entry modeling and analysis techniques. *Proc Int Astron Union* 2(S236):95–106
- Rittmaster R, Adamowicz WL, Amiro B, Pelletier RT (2006) Economic analysis of health effects from forest fires. *Can J For Res* 36(4):868–877. <https://doi.org/10.1139/X05-293>
- Robertson D, Stern E, Mathias D (2017a) Ground Hazards from 100 - 300 m Asteroid Impacts, American Astronomical Society, DPS meeting #49, id.106.01.
- Robertson D, Wheeler L, Mathias D (2017b) Comparison of damage from hydrocode simulations of an asteroid airburst or impact on land, in deep, or in shallow water. *Planetary Defense Conference*.
- Robertson D, Gisler G (2019) Near and far-field hazards of asteroid impacts in oceans. *Acta Astronaut* 156:62–277
- Robertson D, Mathias D (2017) Effect of yield curves and porous crush on hydrocode simulations of asteroid airburst. *J Geophys Res Planets* 122:599–613
- Robertson DK, Mathias DL (2019) Hydrocode simulations of asteroid airbursts and constraints for Tunguska. *Icarus* 327:36–47

- Robock A (2000) Volcanic eruptions and climate. *Rev Geophys* 38(2):191–219. <https://doi.org/10.1029/1998rg000054>
- Rocha YM, de Moura GA, Desidério GA, de Oliveira CH, Lourenço FD, de Figueiredo Nicolette LD (2021) The impact of fake news on social media and its influence on health during the COVID-19 pandemic: a systematic review. *J Public Health Theor Prac*. <https://doi.org/10.1007/s10389-021-01658-z>
- Rose WI, Durant A (2009) Fine ash content of explosive eruptions. *J Volcanol Geothermal Res* 186(1–2):32–39
- Rowe PB, Countryman CM, Storey HC (1949) Probably peak discharge and erosion rates from Southern California watersheds as influenced by fire. Department of Agriculture, Forest Service, Pacific Southwest Forest and Range Experiment Station, Berkeley, California.
- Rumpf CM, Lewis HG, Atkinson PM (2017) Asteroid impact effects and their immediate hazards for human populations. *Geophys Res Lett* 44(8):3433–3440. <https://doi.org/10.1002/2017GL073191>
- Sankey JB, Germino MJ, Glenn NF (2009) Aeolian sediment transport following wildfire in sagebrush steppe. *J Arid Environ* 73(10):912–919. <https://doi.org/10.1016/j.jaridenv.2009.03.016>
- Sankey JB, Glenn NF, Germino MJ, Gironella AIN, Thackray GD (2010) Relationships of aeolian erosion and deposition with LiDAR-derived landscape surface roughness following wildfire. *Geomorphology* 119(1–2):135–145. <https://doi.org/10.1016/j.geomorph.2010.03.013>
- Sankey JB, Germino MJ, Benner SG, Glenn NF, Hoover AN (2012) Transport of biologically important nutrients by wind in an eroding cold desert. *Aeol Res* 7:17–27. <https://doi.org/10.1016/j.aeolia.2012.01.003>
- Sankey JB, Kreidler J, Hawbaker TJ, McVay JL, Miller ME, Mueller ER, Vaillant NM, Lowe SE, Sankey TT (2017) Climate, wildfire, and erosion ensemble foretells more sediment in western USA watersheds. *Geophys Res Lett* 44(17):8884–8892
- Santi P, Rengers FK (2020) Wildfire and Landscape Change in Treatise on Geomorphology. In: John Clague (Eds.) doi <https://doi.org/10.1016/B978-0-12-818234-5.00017-1> p 1–26.
- Sarna-Wojcicki AM, Shipley S, Waitt R, Dzurisin D, Wood SH (1981) Areal distribution, thickness, mass, volume, and grain size of air-fall ash from the six major eruptions of 1980. In: Lipman PW, Christiansen RL (eds) *The 1980 Eruptions of Mount St Helens*. U.S. Government Printing Office, Washington, D.C., pp 577–601
- Schallock J, Brühl C, Bingen C, Höpfner M, Rieger L, Lelieveld J (2021) Radiative forcing by volcanic eruptions since 1990, calculated with a chemistry-climate model and a new emission inventory based on vertically resolved satellite measurements. *Atmos Chem Phys Discuss*. <https://doi.org/10.5194/acp-2021-654>
- Schilling S (2014) Laharz_py: GIS tools for automated mapping of lahar inundation hazard zones USGS open-file report 2014–1073. U.S. Geological Survey, Vancouver, Washington. <https://doi.org/10.3133/ofr20141073>
- Schmidt KM, Hanshaw MN, Howle JF, Kean JW, Staley DM, Stock JD, Bawden GW (2011) Hydrologic conditions and terrestrial laser scanning of post-fire debris flows in the San Gabriel Mountains, CA, U.S.A. In: Genevois R, Hamilton DL, Prestininzi A (eds) *Debris-flow hazards mitigation, mechanics, prediction, and assessment*. Casa Editrice University, pp 583–593
- Schmidt R, Holsapple K (1982) Estimates of crater size for large-body impact: gravity-scaling results Chapter in *Geological implications of impacts of large asteroids and comets on the Earth*. In: Silver and Schultz (eds.) *Geological Society of America*. <https://doi.org/10.1130/SPE190-p93>
- Schuiling R, Cathcart R, Badescu V, Isvoranu D, Pelinovsky E (2007) Asteroid impact in the black sea. Death by drowning or asphyxiation? *Nat Hazards* 40:327–338
- Schulte P, Alegret L, Arenillas I et al (2012) The Chicxulub asteroid impact and mass extinction at the cretaceous-paleogene boundary. *Science* 327(5970):1214
- Schwaiger H, Denlinger R, Mastin LG (2012) Ash3d: a finite-volume, conservative numerical model for ash transport and tephra deposition. *J Geophys Res*. <https://doi.org/10.1029/2011JB008968>
- Schwaiger HF, Iezzi AM, Fee D (2019) AVO-G2S: A modified, open-source ground-to-space atmospheric specification for infrasound modeling. *Comput Geosci* 125:90–97
- Searcy C, Dean K, Stringer W (1998) PUFF: a high-resolution volcanic ash tracking model. *J Volcanol Geoth Res* 80:1–16
- Self S, Rampino MR (1980) The 1883 eruption of Krakatau. *Nature* 292:699–704
- Self S, Zhao J-X, Holasek RE, Torres RC, King AJ (1996) The atmospheric impact of the 1991 Mount Pinatubo Eruption. In: Newhall CG, Punongbayan RS (eds) *Fire and Mud: The eruptions and Lahars of Mount Pinatubo*, Philippines. University of Washington Press, Seattle, pp 1089–1116
- Senkbeil J, Myers L, Jasko S, Reed J, Mueller R (2020) Communication and hazard perception lessons from category five hurricane michael. *Atmosphere* 11:804

- Shabestari K, Yamazaki F (2001) A proposal of instrumental seismic intensity scale compatible with MMI evaluated from three-component acceleration records. *Earthq Spectra* 17(4):711–723
- Shakesby RA (2011) Post-wildfire soil erosion in the Mediterranean: review and future research directions. *Earth Sci Rev* 105(3–4):71–100
- Shakesby RA, Doerr SH (2006) Wildfire as a hydrological and geomorphological agent. *Earth Sci Rev* 74:269–307
- Sheikh PA (2005) The Impact of Hurricane Katrina on Biological Resources, CRS Report for Congress. Order Code RL33117. https://digital.library.unt.edu/ark:/67531/metacrs/7672/m1/1/high_res_d/RL33117_2005Oct18.pdf
- Shuvalov V, Svetsov V, Trubetskaya I (2013) An estimate for the size of the area of damage on the Earth's surface after impacts of 10–300 m asteroids. *Sol Syst Res* 47(4):260–267
- Shuvalov V, Svetsov V, Popova O, Glazachev D (2017) Numerical model of the Chelyabinsk meteoroid as a strengthless object. *Planet Space Sci* 147:38–47
- Sigl M, Winstrup M, McConnell JR, Welten KC, Plunkett G, Ludlow F, Buntgen U, Caffee M, Chellman N, Dahl-Jensen D, Fischer H, Kipfstuhl S, Kostick C, Maselli OJ, Mekhaldi F, Mulvaney R, Muscheler R, Pasteris DR, Pilcher JR, Salzer M, Schupbach S, Steffensen JP, Vinther BM, Woodruff TE (2015) Timing and climate forcing of volcanic eruptions for the past 2500 years. *Nature* 523(7562):543–549. <https://doi.org/10.1038/nature14565>
- Simkin TL, Fiske RS (1983) *Krakatau 1883: the volcanic eruption and its effects*. Smithsonian Institution, Washington D.C, p 464
- Smith HG, Sheridan GJ, Lane PN, Nyman P, Haydon S (2011) Wildfire effects on water quality in forest catchments: a review with implications for water supply. *J Hydrol* 396(1):170–192
- Sparks, RSJ, Self S, Gratten J, Oppenheimer C, Pyle DM, Rymer H (2005) *Supereruptions: global effects and future threats*. Report of a Geological Society Working Group. p.25
- Spence R, Pomonis A, Baxter PJ, Coburn AW, White M, Dayrit M (1995) Building damage caused by the Mount Pinatubo eruption. In: Newhall C, Punongbayan RS (eds) *Fire and Mud: Eruptions and Lahars of Mount Pinatubo, Philippines*. University of Washington Press, Seattle, pp 1055–1062
- Staley DM, Kean JW, Rengers FK (2020) The recurrence interval of post-fire debris-flow generating rainfall in the southwestern United States. *Geomorphol* 370:107392. <https://doi.org/10.1016/j.geomorph.2020.107392>
- Staley DM, Negri JA, Kean JW, Laber JL, Tillery AC, Youberg AM (2017) Prediction of spatially explicit rainfall intensity-duration thresholds for post-fire debris-flow generation in the western United States. *Geomorphol* 278:149–162
- Stanley ML, Barr N, Peters K, Seli P (2021) Analytic-thinking predicts hoax beliefs and helping behaviors in response to the COVID-19 pandemic. *Think Reason* 27(3):464–477. <https://doi.org/10.1080/13546783.2020.1813806>
- Stein AF, Draxler RR, Rolph GD, Stunder BJB, Cohen MD, Ngan F (2015) NOAA's HYSPLIT atmospheric transport and dispersion modeling system. *Bull Am Meteor Soc* 96(12):2059–2077. <https://doi.org/10.1175/BAMS-D-14-00110.1>
- Steinberg L (2004) Cruz A (2004) When natural and technological disasters collide: lessons from the Turkey earthquake of August 17. *Nat Hazard Rev* 5(3):121–130
- Stohl A, Forster C, Frank A, Seibert P, Wotawa G (2005) Technical note: the Lagrangian particle dispersion model FLEXPART version 6.2. *Atmos Chem Phys* 5:2461–2474. <https://doi.org/10.5194/acp-5-2461-2005>
- Stokes GH, Barbee BW, Bottke Jr. WF et al. (2017) Update to determine the feasibility of enhancing the search and characterization of NEOs. National Aeronautics and Space Administration. https://www.nasa.gov/sites/default/files/atoms/files/2017_neo_sdt_final_e-version.pdf
- Stothers RB (1984) The great tambora eruption in 1815 and its aftermath. *Science* 224(4654):1191
- Svetsov V, Shuvalov V (2017) Thermal radiation from impact plumes. *Meteorit Planet Sci* 54(1):126–141
- Svetsov V, Artemieva N, Shuvalov V (2017) Seismic efficiency of meteor airbursts. *Geophys Doklady Earth Sci* 475(2):935–938
- Svetsov V, Shuvalov V, Kosarev I (2020) Formation of Libyan desert glass: numerical simulations of melting silica due to radiation from near-surface airbursts. *Meteorit Planet Sci* 55(4):895–910
- Symons GJ (1888) The eruption of krakatoa and subsequent phenomena. *Q J R Meteorol Soc* 14(68):301–307. <https://doi.org/10.1002/qj.4970146809>
- Taddeucci J, Alatorre-Ibargüengoitia MA, Cruz-Vázquez O, Del Bello E, Scarlato P, Ricci T (2017) In-flight dynamics of volcanic ballistic projectiles. *Rev Geophys* 55(3):675–718. <https://doi.org/10.1002/2017RG000564>
- Ten Brink U, Lee H, Geist E, Twichell D (2010) Assessment of tsunami hazards to the U.S. East Coast using relationships between submarine landslides and earthquakes. *Mar Geol* 264:65–73

- Thomas DSG, Leason HC (2005) Dunefield activity response to climate variability in the southwest Kalahari. *Geomorphol* 64:117–132
- Thomas G, Olivero J (1986) The heights of polar mesospheric clouds. *Geophys Res Lett* 13(13):1403–1406
- Toon OB, Turco RP, Westphal D, Malone R, Liu MS (1988) A multidimensional model for aerosols—description of computational analogs. *J Atmos Sci* 45:2123–2143
- Toon OB, Zahnle K, Morrison D, Turco RP, Covey C (1997) Environmental perturbations caused by the impacts of asteroids and comets. *Rev Geophys* 35(1):41–78. <https://doi.org/10.1029/96RG03038>
- U.S. Army Corps of Engineers (2010) Hydrologic Modeling System, HEC-HMS: User's Manual version 3.5. Institute for Water Resources, Hydrologic Engineering Center, Davis, California.
- U.S. Department of Agriculture, Natural Resources Conservation Service (2009) Small Watershed Hydrology: WinTR-55 User Guide. Conservation Engineering Division
- Ugolnikov O, Maslov I (2019) Polarization analysis and probable origin of bright noctilucent clouds with large particles in June 2018. *Planet Space Sci* 179:104713
- Ulery A, Graham R, Bowen L (1996) Forest fire effects on soil phyllosilicates in California. *Soil Sci Soc Am J* 60(1):309315
- Varekamp JC, Luhr JF, Prestegard KL (1984) The 1982 eruptions of El Chichón volcano (Chiapas, Mexico): character of the eruptions, ash-fall deposits, and gasphase. *J Volcanol Geoth Res* 23(1–2):39–68
- Verbeek, RDM (1885) Krakatau. Batavia (Jakarta), p. 495.
- Vermeire LT, Wester DB, Mitchell RB, Fuhrendorf SD (2005) Fire and grazing effects on wind erosion, soil water content, and soil temperature. *J Environ Qual* 34:1559–1565
- Waitt R (1981) Devastating pyroclastic density flow and attendant air fall of May 18 - Stratigraphy and sedimentology of deposits. In: Lipman PW, Mullineaux DR (eds) The 1980 Eruptions of Mount St Helens, Washington U.S. Geological Survey Professional Paper 1250. US Government Printing Office, Washington, D.C., pp 438–458
- Wald D, Quitoriano V, Heaton T, Kanamori H (1999) Relationships between peak ground acceleration, peak ground velocity, and modified Mercalli intensity in California. *Earthq Spectra* 15(3):557–564. <https://doi.org/10.1193/1.1586058>
- Wang G, Li J, Ravi S, et al. (2019) Post-fire redistribution of soil carbon and nitrogen at a grassland-shrubland ecotone. *Ecosyst* 22:174–188. <https://doi.org/10.1007/s10021-018-0260-2>
- Warrick RA, Anderson J, Lyons J, Ressler J, Mary W, Warrick T (1981) Four Communities under Ash after Mount St. Helens. Program on Technology, Environment, and Man, Monograph #34. Institute of Behavioral Science, University of Colorado, Boulder, CO, p. 143.
- Weidner E, Todd A (2011). From the forest to the faucet: Drinking water and forests in the US. Methods paper, ecosystem services and markets program area, State and Private Forestry. USDA Forest Service. [Available at http://www.fs.fed.us/ecosystemservices/pdf/forests2faucets/F2F_Methods_Final.pdf.]
- Wheeler LF, Mathias DL (2019) Probabilistic assessment of tunguska-scale asteroid impacts. *Icarus* 327:83–96. <https://doi.org/10.1016/j.icarus.2018.12.017>
- Wheeler L, Register P, Mathias D (2017) A fragment-cloud model for asteroid breakup and atmospheric energy deposition. *Icarus* 295:149–169
- Wheeler L, Mathias D, Stokan E, Brown P (2018) Atmospheric energy deposition modeling and inference for varied meteoroid structures. *Icarus* 315:79–91
- Whicker JE, Pinder DD (2006) Breshears Increased wind erosion from forest wildfire: implications for contaminant-related risks. *J Environ Qual* 35:468–478
- Whicker JJ, Breshears DD, Wasiolek PT, Kirchner TB, Tavani RA, Schoep DA, Rodgers JC (2002) Temporal and spatial variation of episodic wind erosion in unburned and burned semi-arid shrubland. *J Environ Qual* 31:599–612
- Wiggs GF, Livingstone I, Thomas DSG, Bullard JE (1994) Effect of vegetation removal on airflow patterns and dynamics in the southwest Kalahari desert. *Land Degrad Rehabil* 5:13–24
- Wiggs GF, Livingstone I, Thomas DSG, Bullard JE (1996) Airflow and roughness characteristics over partially vegetated linear dunes in the southwest Kalahari desert. *Earth Surf Proc Land* 21:19–34
- Wiggs GF, Thomas DSG, Bullard JE, Livingstone I (1995) Dune mobility and vegetation cover in the southwest Kalahari. *Earth Surf Proc Land* 20:515–529
- Wilder BA, Lancaster JT, Cafferata PH, Coe DB, Swanson BJ, Lindsay DN, Kinoshita AM (2021) An analytical solution for rapidly predicting post-fire peak streamflow for small watersheds in southern California. *Hydro Process* 35(1):e13976. <https://doi.org/10.1002/hyp.13976>
- Wilson L, Sparks RSJ, Huang TC, Watkins ND (1978) The control of volcanic column heights by eruption energetics and dynamics. *J Geophys Res* 83(B4):1829–1836. <https://doi.org/10.1029/jb083ib04p01829>

- Wilson TM, Stewart C, Sword-Daniels V, Leonard GS, Johnston DM, Cole JW, Wardman J, Wilson G, Barnard ST (2012) Volcanic ash impacts on critical infrastructure. *Phys Chem Earth Parts A B C* 45:5–23
- Witchell W (1938) A photograph of the royal naval college, greenwich, taken at midnight of June 30, 1908, the northern sky being then brightly illuminated as an after effect of the fall of the great siberian meteor. *Q J R Meteorol Soc* 64:612
- Wolbach WS, Gilmour I, Anders E, Sharpton VL, Ward PD (1990) Major wildfires at the Cretaceous/Tertiary boundary. In: *Global Catastrophes in Earth History; An Interdisciplinary Conference on Impacts, Volcanism, and Mass Mortality. Geological Society of America*, <https://doi.org/10.1130/SPE247-p391>
- Worden CB, Wald DJ, Allen TI, Lin K, Garcia D Cua G (2010) A revised ground-motion and intensity interpolation scheme for shakemap. *Bull Seismol Soc Am* 100(6):3083–3096
- Worthington A, Cole R (1900) Impact with a liquid surface studied by the aid of instantaneous photography Paper II. *Philos Transact Royal Soc London Series A* 194:175–199
- Wünnemann K, Weiss R, Hofmann K (2010) Characteristics of ocean impact-induced large water waves—re-evaluation of the tsunami hazard. *Meteorit Planet Sci* 42(11):1893–1903
- Zender CS, Bian H, Newman D (2003) Mineral dust entrainment and deposition (DEAD) model description and 1990s dust climatology. *J Geophys Res Atmos*. <https://doi.org/10.1029/2002JD002775>
- Zenkin G, Ilyin A (1964) On the radiant burn of trees in the Tunguska meteorite explosion area. *Meteoritika* 24:129–140 (**In Russian**)
- Zhang S, Matsushimab T (2018) Numerical investigation of debris materials prior to debris flow hazards using satellite images. *Geomorphology* 308:54–63
- Zhang L, Zhang S, Huang R (2014) Multi-hazard scenarios in Beichuan, China: the first five years after the 2008 Wenchuan earthquake. *Eng Geol* 180:4–20
- Zhu et al (2021) Warning decision-making for landslide dam breaching flood using influence diagrams. *Front Earth Sci*. <https://doi.org/10.3389/feart.2021.679862>
- Zobeck TM, Fryrear DW, Pettit RD (1989) Management effects on wind-eroded sediment and plant nutrients. *J Soil Water Conserv* 44:160–163

Publisher's Note Springer Nature remains neutral with regard to jurisdictional claims in published maps and institutional affiliations.

Springer Nature or its licensor (e.g. a society or other partner) holds exclusive rights to this article under a publishing agreement with the author(s) or other rightsholder(s); author self-archiving of the accepted manuscript version of this article is solely governed by the terms of such publishing agreement and applicable law.